

1.3.2.1

NACA TN 2168

# NATIONAL ADVISORY COMMITTEE FOR AERONAUTICS

TECHNICAL NOTE 2168

EXPERIMENTAL INVESTIGATION OF THE  
EFFECT OF VERTICAL-TAIL SIZE AND LENGTH AND OF FUSELAGE  
SHAPE AND LENGTH ON THE STATIC LATERAL STABILITY  
CHARACTERISTICS OF A MODEL WITH  $45^\circ$  SWEPTBACK  
WING AND TAIL SURFACES

By M. J. Queijo and Walter D. Wolhart

Langley Aeronautical Laboratory  
Langley Air Force Base, Va.

**DISTRIBUTION STATEMENT A**  
Approved for Public Release  
Distribution Unlimited



Washington

August 1950

**Reproduced From  
Best Available Copy**

20000801 116

DTIC QUALITY INSPECTED 4

AQM00-10-3339

NATIONAL ADVISORY COMMITTEE FOR AERONAUTICS

---

TECHNICAL NOTE 2168

---

EXPERIMENTAL INVESTIGATION OF THE  
EFFECT OF VERTICAL-TAIL SIZE AND LENGTH AND OF FUSELAGE  
SHAPE AND LENGTH ON THE STATIC LATERAL STABILITY  
CHARACTERISTICS OF A MODEL WITH  $45^\circ$  SWEPTBACK  
WING AND TAIL SURFACES

By M. J. Queijo and Walter D. Wolhart

SUMMARY

An investigation was made to determine the effects of vertical-tail size and length and of fuselage shape and length on the lateral static stability characteristics of a model with wing and vertical tails having the quarter-chord lines swept back  $45^\circ$ . The results indicate that the directional instability of the various isolated fuselages was about two-thirds as large as that predicted by classical theory. A reduction in area of vertical tails (geometric aspect ratio kept constant) attached to a given fuselage resulted in an increase in the effective aspect ratio of the vertical tail for the range of tail sizes considered. Simple analytical considerations indicate, however, that for tail sizes below the range investigated, the opposite effect would be expected.

For the fuselage-tail combinations investigated, the tail effectiveness usually decreased with increasing angle of attack, with the greatest rate of decrease occurring at angles of attack greater than about  $16^\circ$ .

The wing-fuselage interference for the midwing arrangements investigated was only slightly affected by the shape of the fuselage and tended to increase slightly the directional stability of the combination. The interference effects of the wing tended to decrease the vertical-tail effectiveness, particularly at high angles of attack. The large effects observed were attributed to a partially stalled condition of the wing.

Preceding Page's Blank

## INTRODUCTION

Recent advances in the understanding of the principles of high-speed flight have led to significant changes in the design of the principal components of airplanes. Two of the more important changes have been the incorporation of large amounts of sweep of the wing and tail surfaces and the elevation of the horizontal tail to a higher position. Much information is available on the influence of the wing, fuselage, and tail geometry on the static stability characteristics of the more conventional airplane designs (for example, references 1 and 2); however, little information is available on the influence of the various airplane components on the characteristics of airplanes having wings and tail surfaces with large amounts of sweep. In order to provide such information, a series of investigations is being conducted in the Langley stability tunnel with a model having various interchangeable parts. The effects of changes in the size and location of the horizontal tail on the low-speed static lateral stability characteristics have been reported in reference 3. The effects on the static-lateral-stability derivatives of variations of vertical-tail size and length and of fuselage shape and length are presented herein. The data also have been used to determine interference effects between the wing and fuselage and the interference effects of the wing-fuselage combination on the vertical-tail effectiveness.

## SYMBOLS AND COEFFICIENTS

The data presented herein are in the form of standard NACA coefficients of forces and moments which are referred to the stability axes, with the origin at the projection on the plane of symmetry of the quarter-chord point of the mean aerodynamic chord or at the midpoint of the fuselage. The positive directions of the forces, moments, and angular displacements are shown in figure 1. The coefficients and symbols are defined as follows:

A	aspect ratio ( $b^2/S$ )
b	span, measured perpendicular to fuselage center line, feet
c	chord, measured parallel to plane of symmetry, feet
$c_r$	root chord, feet
$c_t$	tip chord, feet

$\bar{c}$	wing mean aerodynamic chord, feet $\left( \bar{c}_W = \frac{2}{S_W} \int_0^{b_W/2} c_W^2 dy \right)$
$D_F$	fuselage diameter at longitudinal station of aerodynamic center of vertical tail, feet
$l$	fuselage length, feet
$l_V$	tail length, distance from origin of axis $l/2$ to $\bar{c}/4$ of vertical tail, feet
$q$	dynamic pressure, pounds per square foot $\left( \frac{1}{2} \rho V^2 \right)$
$S$	area, square feet
$S_S$	projected side area of fuselage, square feet
$t$	maximum thickness of fuselage, feet
$V$	velocity, feet per second
$V_F$	volume of fuselage, cubic feet
$x$	chordwise distance from leading edge of root chord to quarter-chord point of any chord, feet
$\bar{x}$	chordwise distance from leading edge of root chord to quarter-chord point of mean aerodynamic chord, feet $\left( \bar{x}_W = \frac{2}{S_W} \int_0^{b_W/2} c_W x_W dy \right)$
$y$	spanwise distance measured from the plane of symmetry, feet
$\bar{y}$	spanwise distance to quarter chord of mean aerodynamic chord, feet $\left( \bar{y}_W = \frac{2}{S_W} \int_0^{b_W/2} c_W y_W dy \right)$
$z_V$	perpendicular distance from fuselage center line to aerodynamic center of vertical tail, feet
$\alpha$	angle of attack, degrees

$\lambda$	taper ratio $\left(\frac{c_t}{c_r}\right)$
$\eta_Y, \eta_N$	angle-of-attack correction factors to effectiveness of vertical tail in yaw
$\Lambda$	angle of sweepback of quarter-chord line, degrees
$\rho$	mass density, slugs per cubic foot
$\psi$	angle of yaw, degrees
$C_L$	lift coefficient $\left(\frac{\text{Lift}}{qS_W}\right)$
$C_D$	drag coefficient $\left(\frac{\text{Drag}}{qS_W}\right)$ ; $C_D = -C_X$ at $\psi = 0^\circ$
$C_X$	longitudinal-force coefficient $\left(\frac{\text{Longitudinal force}}{qS_W}\right)$
$C_Y$	lateral-force coefficient $\left(\frac{\text{Lateral force}}{qS_W}\right)$
$C_m$	pitching-moment coefficient $\left(\frac{\text{Pitching moment}}{qS_W \bar{c}_W}\right)$
$C_n$	yawing-moment coefficient $\left(\frac{\text{Yawing moment}}{qS_W b_W}\right)$
$C_l$	rolling-moment coefficient $\left(\frac{\text{Rolling moment}}{qS_W b_W}\right)$
$C_{Y_\psi}$	$C_{Y_\psi} = \left(\frac{\partial C_Y}{\partial \psi}\right)_{\psi=0^\circ}$
$C_{l_\psi}$	$C_{l_\psi} = \left(\frac{\partial C_l}{\partial \psi}\right)_{\psi=0^\circ}$

$$C_{n_\psi} = \left( \frac{\partial C_n}{\partial \psi} \right)_{\psi=0^\circ}$$

$$(C_{L_\alpha})_V = \left( \frac{\partial (C_L)_V}{\partial \alpha} \right)_{\alpha=0^\circ}, \text{ where } (C_L)_V \text{ is based on vertical-tail area}$$

$$\left. \begin{array}{l} \Delta_1 C_{Y_\psi}, \Delta_1 C_{n_\psi}, \\ \Delta_1 C_{l_\psi} \end{array} \right\} \begin{array}{l} \text{increments of coefficients caused by wing-fuselage inter-} \\ \text{ference; that is, } \Delta_1 C_{Y_\psi} = (C_{Y_\psi})_{W+F} - (C_{Y_\psi})_W - (C_{Y_\psi})_F \end{array}$$

$$\left. \begin{array}{l} \Delta_2 C_{Y_\psi}, \Delta_2 C_{n_\psi}, \\ \Delta_2 C_{l_\psi} \end{array} \right\} \begin{array}{l} \text{increments of coefficients caused by wing-fuselage inter-} \\ \text{ference on vertical-tail effectiveness; that is,} \\ \Delta_2 C_{Y_\psi} = [(C_{Y_\psi})_{W+F+V} - (C_{Y_\psi})_{W+F}] - [(C_{Y_\psi})_{F+V} - (C_{Y_\psi})_F] \end{array}$$

Subscripts and abbreviations:

W	wing
V	vertical tail; used with subscripts 1 to 5 to denote the various vertical tails (see fig. 2)
F	fuselage; used with subscripts 1 to 5 to denote the various fuselages (see fig. 3)
S	slat
e	effective
s	side area

#### APPARATUS AND TESTS

All parts of the models used in this investigation were constructed of mahogany. Sketches of the parts of the models are presented as figures 2, 3, and 4. The various vertical tails and fuselages will be referred to henceforth by the symbol and number assigned to them in figures 2 and 3. All vertical tails had  $45^\circ$  sweepback of the quarter-chord line, taper ratio of 0.6, and NACA 65A008 profiles (table I) in planes parallel to the fuselage center line. The ratios of tail area to wing area were chosen to cover a range representative of that used for

current high-speed airplane configurations. The tails were mounted on the fuselages so that the tail length was always a constant percent of the fuselage length ( $\frac{l_T}{l} = 0.42$ ). The tail length was varied by changing the fuselage length. The three fuselages (fineness ratios of 5.0, 6.67, and 10.0) of circular-arc profile used in the investigation are shown in figure 3. Two additional fuselages having the same fineness ratio as fuselage 2 (fineness ratio of 6.67) were used to determine the effects of fuselage nose and trailing-edge modifications. All fuselages had circular cross sections and all had the same maximum thickness. The coordinates of the fuselages are given in table II.

The wing had an aspect ratio of 4.0, taper ratio of 0.6, sweepback of  $45^\circ$  of the quarter-chord line, and NACA 65A008 profiles parallel to the plane of symmetry. The wing was mounted on the fuselage so that the quarter-chord point of the mean aerodynamic chord coincided with the fuselage mounting point (fig. 4). A summary of the geometric characteristics of the various model components is given in table III. A full-span slat, fitted to the wing for some tests with fuselage  $F_2$ , had a chord which was 8 percent of the wing chord. (See fig. 4.) The slat was made by bending a strip of  $\frac{1}{16}$ -inch-thick aluminum sheet to fit the contour of the wing leading edge. Photographs of some of the model configurations are presented as figure 5.

Most of the tests of this investigation were conducted in the 6-foot-diameter rolling-flow test section of the Langley stability tunnel. Tests of configurations with fuselages  $F_4$  and  $F_5$  were conducted in the 6- by 6-foot curved-flow test section of the Langley stability tunnel. All tests were made at a dynamic pressure of 24.9 pounds per square foot, which corresponds to a Mach number of 0.13 and a Reynolds number of  $0.71 \times 10^6$  based on the wing mean aerodynamic chord. The angle of attack of the model was varied from about  $-4^\circ$  to approximately  $32^\circ$  for yaw angles of  $0^\circ$  and  $\pm 5^\circ$ .

#### CORRECTIONS

The angle of attack, longitudinal-force coefficient, and rolling-moment coefficient have been corrected for jet-boundary effects. No corrections have been applied for the effects of blocking, turbulence, or support-strut interference. At relatively large angles of attack (above about  $20^\circ$ ) the vertical tail generally was in the wake of the support strut; hence, data dependent principally on the vertical-tail contribution probably are unreliable at angles of attack above about  $20^\circ$ .

This unreliability is particularly true for data obtained with fuselage  $F_3$ , and therefore these data are not presented.

#### METHODS OF ANALYSIS

The results of the present investigation are analyzed in terms of the individual contributions of the various parts and the more important interference effects. In accordance with conventional procedures (for example, see reference 2) the static-lateral-stability derivatives of a complete airplane can be expressed as:

$$C_{Y_\psi} = (C_{Y_\psi})_F + (C_{Y_\psi})_W + (C_{Y_\psi})_V + \Delta_1 C_{Y_\psi} + \Delta_2 C_{Y_\psi} \quad (1)$$

$$C_{n_\psi} = (C_{n_\psi})_F + (C_{n_\psi})_W + (C_{n_\psi})_V + \Delta_1 C_{n_\psi} + \Delta_2 C_{n_\psi} \quad (2)$$

$$C_{l_\psi} = (C_{l_\psi})_F + (C_{l_\psi})_W + (C_{l_\psi})_V + \Delta_1 C_{l_\psi} + \Delta_2 C_{l_\psi} \quad (3)$$

The subscripts F and W refer to the derivatives of the isolated fuselage and of the isolated wing, respectively. In the general case, the subscript V refers to the contribution of the vertical tail when mounted on the fuselage and when in the presence of the horizontal tail. The present tests were made without a horizontal tail, since the effects of various horizontal-tail sizes and locations were investigated in reference 3. In the present paper, therefore, the derivatives with the subscript V include both the effectiveness of the isolated vertical tail and the interference of the fuselage.

The vertical-tail contribution can be expressed analytically as follows:

$$(C_{Y_\psi})_V = (C_{L_\alpha})_V \frac{S_V}{S_W} \eta_Y \quad (4)$$

$$(C_{n_\psi})_V = -(C_{L_\alpha})_V \frac{l_V}{b_W} \frac{S_V}{S_W} \eta_N \quad (5)$$



$$(C_{l_{\psi}})_V = \left( \frac{z_V}{b_W} \cos \alpha - \frac{l_V}{b_W} \sin \alpha \right) \frac{S_V}{S_W} (C_{L_{\alpha}})_V \quad (6)$$

where  $(C_{L_{\alpha}})_V$  is the effective vertical-tail lift-curve slope when the model is at zero angle of attack, and  $\eta_Y$  and  $\eta_N$  are correction factors which account for the variation in tail effectiveness with angle of attack. (A similar correction to  $C_{l_{\psi}}$  is neglected because it generally has been found to be very nearly 1.0.) Equations (4) to (6) are similar to equations given in reference 4, except that in the reference the factors  $\eta_Y$  and  $\eta_N$  are neglected. The results of the present tests are used for evaluating the factors  $\eta_Y$  and  $\eta_N$  and the effective aspect ratio  $A_{eV}$ , corresponding to the vertical-tail lift-curve slope  $(C_{L_{\alpha}})_V$ .

Perhaps the most consistent approach to the problem of evaluating tail effectiveness would involve determination of  $A_{eV}$  corresponding to  $(C_{L_{\alpha}})_V$  as determined from equation (4). In order to make use of such values of  $A_{eV}$  in the calculation of  $(C_{n_{\psi}})_V$  and  $(C_{l_{\psi}})_V$ , effective, rather than geometric, values of the tail length  $l_V$  and of the tail height  $z_V$  also would have to be known. From practical considerations, it has seemed most convenient to assume that the location of the vertical-tail center of pressure is given accurately by the geometric lengths  $l_V$  and  $z_V$ . Since the directional-stability parameter  $(C_{n_{\psi}})_V$  is considered to be the most important of the three static-lateral-stability parameters, values of  $A_{eV}$ , corresponding to  $(C_{L_{\alpha}})_V$  as determined from equation (5), are obtained in the present analysis. The reliability of values of  $A_{eV}$  so determined, when used to calculate  $(C_{Y_{\psi}})_V$  and  $(C_{l_{\psi}})_V$ , is checked against the experimental results.

Since, at zero angle of attack, the factor  $\eta_N$  is 1.0, equation (5) can be rewritten as

$$(C_{L_{\alpha}})_V = -\frac{b_W S_W}{l_V S_V} (C_{n_{\psi}})_V$$

Values of  $A_{eV}$ , corresponding to  $(C_{L_{\alpha}})_V$ , may be obtained from theory such as that of reference 5. A correction to  $A_{eV}$  for the effect of the horizontal tail can be obtained from reference 3.

The increments prefixed by  $\Delta_1$  and  $\Delta_2$  express, respectively, the interference of the wing-fuselage combination and the interference of the wing-fuselage on the vertical-tail effectiveness; for example,

$$\Delta_1 C_{Y_\psi} = (C_{Y_\psi})_{W+F} - [(C_{Y_\psi})_W + (C_{Y_\psi})_F]$$

and

$$\Delta_2 C_{Y_\psi} = [(C_{Y_\psi})_{W+F+V} - (C_{Y_\psi})_{W+F}] - [(C_{Y_\psi})_{F+V} - (C_{Y_\psi})_F]$$

The interference increments usually are assumed to apply to airplanes having configurations which are somewhat similar to that of the model used in evaluating the increments. Of the various factors which affect the magnitudes of the interference increments, the height of the wing, relative to the center line of the fuselage, previously has been found to be one of the most important (reference 2). Since, for the present investigation, the wing was located on the center line of the fuselages, the results are considered applicable only to midwing or near-midwing arrangements.

## RESULTS AND DISCUSSION

### Presentation of Results

The basic data obtained in this investigation are presented in figures 6 to 14. The longitudinal characteristics of the wing alone and of the wing with slat are given in figure 6. The static-lateral-stability parameters of the various configurations investigated are given in figures 7 to 14. A summary of the configurations investigated and of the figures that give data for these configurations is given in table IV. Most of the remaining figures (figs. 15 to 30) were made up from the data of figures 7 to 14 and present the data in a form more suitable for analysis.

### Wing Characteristics

The longitudinal aerodynamic characteristics of the wing alone (fig. 6) have been given in reference 3; hence, they are reviewed only briefly in this paper. The plain wing stalled at about  $24^\circ$  angle of attack ( $C_L = 1.0$ ) and showed an aerodynamic-center position of  $0.25\bar{c}_w$ .

The theory of reference 5 predicts an aerodynamic-center position of  $0.26\bar{c}_w$ . Addition of the  $0.08c_w$  slat delayed the stall to about  $26^\circ$  angle of attack ( $C_L = 1.1$ ) but had no appreciable effect on the position of the aerodynamic center at low angles of attack. The slat caused an appreciable reduction in drag at angles of attack greater than about  $8^\circ$ .

Many of the aerodynamic parameters of a complete airplane are dependent to some extent on the character of the flow over the wing; hence, some consideration must be given to the angle-of-attack range over which flow does not separate from the wing. As pointed out in reference 6, an indication of the limit of this range can be obtained by locating the

initial break in the plot of  $C_D - \frac{C_L^2}{\pi A_w}$  against angle of attack. A plot of this increment for the plain wing and for the wing with slat is given in figure 15. The figure shows breaks in the curves at about  $7.7^\circ$  and at about  $16^\circ$  for the wing alone and for the wing with slat, respectively. Corresponding breaks in the curves of the aerodynamic characteristics of combinations involving the wing and the wing with slat are to be expected at about these same angles of attack.

Investigations involving Reynolds number as a variable have shown that for smooth wings increases in Reynolds number tended to extend the angle-of-attack range before which initial breaks occurred in plots of aerodynamic parameters against angle of attack. For this reason results obtained for configurations with slats might be expected to be somewhat similar to data for the plain wing at a higher Reynolds number than the test Reynolds number.

### Fuselage Characteristics

The important characteristics of the various fuselages are summarized in figure 16. In general, the parameters considered  $(C_{Y_\psi})_F$  and  $(C_{n_\psi})_F$  varied only slightly with angle of attack, and therefore the analysis has been limited to characteristics at  $\alpha = 0^\circ$ .

In order that the results obtained may be applied conveniently to arbitrary airplane configurations, coefficients in terms of fuselage dimensions rather than wing dimensions are needed. This manner of expressing the coefficient is accomplished by plotting the quantities

$(C_{Y_\psi})_F \frac{S_w}{S_s}$  and  $(C_{n_\psi})_F \frac{S_w b_w}{V_F}$  against fuselage fineness ratio. The

quantities plotted, therefore, are effectively a lateral-force coefficient based on fuselage side area  $S_s$  and a yawing-moment coefficient based on fuselage volume  $V_F$ .

Comparisons are made with the theory presented in reference 7. Although the theory, which is based on potential-flow considerations, predicts no side force, the experimental results show a positive side force which increases as the fineness ratio is decreased. The variations in fuselage shape considered, for a constant fineness ratio, have a negligible effect on the value of a lateral-force coefficient based on fuselage side area.

The experimental results obtained for the directional-stability parameter  $(C_{n\psi})_F$  of the biconvex fuselages show about the same trend with variation in fineness ratio as that predicted by theory, although, quantitatively, the magnitude is only about two-thirds of that predicted by theory. For a constant fineness ratio, the variations in fuselage shape considered produced a rather large change in the magnitude of the directional-stability parameter based on fuselage volume. An increase in volume near the fuselage nose increased this parameter; whereas an increase in volume over the rear half of the fuselage decreased this parameter.

#### Vertical-Tail Effectiveness

Effective aspect ratio.- As explained in the section entitled "Methods of Analysis," the effective aspect ratio of the vertical tail is obtained by calculating the tail lift-curve slope from experimental values of  $(C_{n\psi})_V$  and then obtaining the corresponding aspect ratio from a theory of plain wings. The theory of reference 5 has been used herein, although it is realized that a swept vertical tail represents an unsymmetrical configuration to which the theory is not strictly applicable. The relationship, given by reference 5, between lift-curve slope and aspect ratio for wings having a sweep angle of  $45^\circ$  and a taper ratio of 0.6 is reproduced in figure 17. The results of the effective-aspect-ratio determinations are presented in figure 18 in the form of the ratio  $A_{eV}/A_V$  plotted against  $b_V/D_F$  for  $\alpha = 0^\circ$ . The quantity  $b_V/D_F$  is the ratio of vertical-tail span to the fuselage diameter at the longitudinal location of the vertical-tail aerodynamic center and is regarded as a significant parameter for determining the influence of the fuselage on the vertical-tail effectiveness. An average curve is drawn through the data obtained with the tails of aspect ratio 1.0; and another curve, through the two points obtained with the tails of aspect ratio 2.0. The fairing of the average curve at low values of  $b_V/D_F$  has been guided by the shape of the calculated curve which represents reasonable maximum values of  $A_{eV}/A_V$  for given values of  $b_V/D_F$ . The calculated curve was determined by an equation derived on the assumption that the fuselage

acts as an infinite end plate on the portion of the vertical tail protruding outside the fuselage. The equation of the curve is

$$\frac{A_{ev}}{A_v} = \frac{2 \left( 2 \frac{b_v}{D_F} - 1 \right)}{2 \frac{b_v}{D_F} - \frac{1 - \lambda_v}{1 + \lambda_v}} \quad (7)$$

A reduction in area (geometric aspect ratio kept constant) of vertical tails attached to a given fuselage resulted in an increase in the effective aspect ratios of the vertical tails for the range of tail size investigated. The calculated curve indicates that for smaller tails the opposite would be true.

The experimental data show that the ratio  $A_{ev}/A_v$  approaches the value 1.0 as  $b_v/D_F$  becomes large. This variation is to be expected since an increase in  $b_v/D_F$  represents a decrease in the size of the end plate relative to the vertical tail. For very large values of  $b_v/D_F$ , the effective and geometric aspect ratios should be approximately equal. The values of  $A_{ev}/A_v$  given in figure 18 depend to some extent on the curve of  $C_{L_\alpha}$  against  $A$  from which the values of  $A_{ev}$  were obtained. The values of  $A_{ev}$  might have been slightly different had some variation of  $C_{L_\alpha}$  with  $A$  other than that of reference 5 been used. The data show some scatter at low values of  $b_v/D_F$ ; this scatter indicates that factors other than  $b_v/D_F$  enter into the determination of  $A_{ev}/A_v$ . The vertical-tail contributions to  $C_{Y_\psi}$  and  $C_{N_\psi}$  at  $\alpha = 0^\circ$  are shown in figure 19. Also shown in the figure are calculated curves of the parameters as determined by equations (4) and (5) and the use of average values of  $A_{ev}$  to determine  $(C_{L_\alpha})_v$ . Ratios of  $A_{ev}/A_v$  of 1.25 and 1.45 were used for vertical tails having geometric aspect ratios of 1.0 and 2.0, respectively. The fact that reasonably good agreement between the calculated curves and the experimental values of  $C_{N_\psi}$  was obtained is of only incidental interest, since the experimental results shown were originally used to determine appropriate values of the ratio  $A_{ev}/A_v$ . The scatter of the experimental points is indicative, however, of the accuracy that might be expected by use of average values of  $A_{ev}/A_v$  for arbitrary arrangements. The agreement between the calculated and experimental values of  $(C_{Y_\psi})_v$  also is reasonably good. Therefore, the values

of  $A_{eV}/A_V$  calculated from increments of  $(C_{n\psi})_V$  appear to be usable for predicting  $(C_{Y\psi})_V$  with reasonable accuracy at least for the arrangements investigated.

The vertical-tail contribution to the derivative  $C_{l\psi}$  can be separated into two parts as given by the two terms of the following equation:

$$(C_{l\psi})_V = \frac{z_V}{b_W} \frac{S_V}{S_W} (C_{L\alpha})_V \cos \alpha - \frac{l_V}{b_W} \frac{S_V}{S_W} (C_{L\alpha})_V \sin \alpha$$

For small angles of attack the equation can be written as

$$(C_{L\alpha})_V = \frac{z_V}{b_W} \frac{S_V}{S_W} (C_{L\alpha})_V - \frac{l_V}{b_W} \frac{S_V}{S_W} (C_{L\alpha})_V \frac{\alpha}{57.3}$$

The first part of the equation is the increment of  $(C_{l\psi})_V$  at  $\alpha = 0^\circ$ , and the second part shows that the variation of  $(C_{l\psi})_V$  with  $\alpha$  is given by

$$\frac{\partial (C_{l\psi})_V}{\partial \alpha} = - \frac{l_V}{b_W} \frac{S_V}{S_W} \frac{(C_{L\alpha})_V}{57.3}$$

In analyzing the contribution of the vertical tail to  $C_{l\psi}$ , consideration has been given to the increment of  $(C_{l\psi})_V$  at zero angle of attack and the rate of change of  $(C_{l\psi})_V$  with angle of attack. The experimental and calculated results for both of these effects are shown in figure 20 to be in fairly good agreement.

Angle-of-attack correction.— In the preceding section, the effective aspect ratio of the vertical tail mounted on the fuselage was determined at zero angle of attack. The effects of variations in angle of attack are now evaluated in terms of the correction factors to the vertical-tail contribution to  $C_{Y\psi}$  and  $C_{n\psi}$ ,  $\eta_Y$  and  $\eta_N$ , respectively.

The variation of the factor  $\eta_Y$  with angle of attack is shown in figure 21 for three values of the ratio  $l_V/b_W$ . In each case an average curve is drawn through the data. The ratios  $l_V/b_W$  and  $S_V/S_W$  seem to

cause no appreciable change in the variation of  $\eta_Y$  with  $\alpha$  for values of  $\alpha$  less than  $6^\circ$ . At higher angles of attack, however, both  $l_V/b_W$  and  $S_V/S_W$  appear to affect the variation of  $\eta_Y$  with  $\alpha$ , but not enough data were available to establish a definite relation between the various parameters. The effects of fuselage shape and vertical-tail aspect ratio on the variation of  $\eta_Y$  with  $\alpha$  are shown in figure 22. Also given in the figure is the average curve from figure 21(b). It is seen that the curve fits the data reasonably well and that the variations in fuselage shape considered have very little effect on the variation of  $\eta_Y$  with  $\alpha$ . Changes in vertical-tail aspect ratio appear to have some effect on the variation of  $\eta_Y$  with  $\alpha$ ; nevertheless, the general trend shown by the average curve is still fairly accurate.

In general, it appears that the vertical-tail contribution to  $C_{Y\psi}$  may be reduced as much as twenty percent as the angle of attack is increased from  $0^\circ$  to  $15^\circ$  and that this reduction usually increases rapidly at higher angles of attack.

The variation of the factor  $\eta_N$  with  $\alpha$  is shown in figure 23 for several values of  $l_V/b_W$  and  $S_V/S_W$ . Average curves are drawn through each set of data. At low angles of attack the area ratio  $S_V/S_W$  appears to have a negligible effect on the variation of  $\eta_N$  with  $\alpha$ ; however, it does have a large effect at angles of attack greater than about  $8^\circ$  and the effects increase with an increase of the  $l_V/b_W$  ratio. Fuselage shape and vertical-tail aspect ratio appear to have some effect on the variation of  $\eta_N$  with  $\alpha$  (fig. 24), but the effects are not clearly defined by the data. In general, the average curve of figure 23(b) fits the data of figure 24 reasonably well.

Except for the smallest vertical tail ( $V_1$ ), the tail contributions to  $C_{N\psi}$  tend to show a smaller decrease with angle of attack than had previously been noted for the tail contribution to  $C_{Y\psi}$ .

### Interference Effects

Wing-fuselage interference.— The lateral-stability data of this investigation were used to determine wing-fuselage interference increments by the procedure explained under "Methods of Analysis." The increments are presented in figure 25 as functions of the angle of attack. Both  $\Delta_1 C_{Y\psi}$  and  $\Delta_1 C_{l\psi}$  show large variations with angle of attack and are of large magnitude at high angles of attack. The increment  $\Delta_1 C_{N\psi}$  is rather small for all fuselage shapes investigated and tends to increase slightly

the directional stability of the wing-fuselage combination over most of the angle-of-attack range. The average value of  $\Delta_1 C_{n_\psi}$  is about  $-0.0002$  up to  $16^\circ$  angle of attack.

Wing-fuselage interference on vertical-tail effectiveness.-

Increments of  $\Delta_2 C_{Y_\psi}$ ,  $\Delta_2 C_{n_\psi}$ , and  $\Delta_2 C_{l_\psi}$  are shown in figures 26, 27, and 28, respectively, for various combinations of the circular-arc fuselages and the vertical tails of aspect ratio 1.0. The data are divided into groups of constant  $l_V/b_W$  ratio. An average curve was drawn through each set of data. In general, the data show little scatter about the faired curves. The addition of the wing almost invariably reduced the tail contribution to the directional stability for the arrangements investigated (fig. 27). The effect was negligible at very small angles of attack, but at  $20^\circ$  angle of attack a value of  $\Delta_2 C_{n_\psi}$  of about 0.0020 was obtained with the largest fuselage ( $F_3$ ). The large interference effects noted at high angles of attack probably result from the partially stalled condition of the wing at these attitudes. If stalling could be avoided, the interference effects undoubtedly would be considerably smaller.

The effects of fuselage shape on the increments of  $C_{Y_\psi}$ ,  $C_{n_\psi}$ , and  $C_{l_\psi}$  caused by wing-fuselage interference on the vertical-tail effectiveness are indicated in figure 29. Also given in the figure are the average curves of the  $\frac{l_V}{b_W} = 0.464$  data of figures 26(b), 27(b), and 28(b). The figure indicates that variations in fuselage shapes considered have little effect on the interference increments and that the average curves fit the data quite well.

A comparison is given in figure 30 between the interference increments  $\Delta_1 C_{n_\psi}$  and  $\Delta_2 C_{n_\psi}$  for a model configuration with and without the wing slat. The model configuration was made up of the wing, fuselage  $F_2$ , and vertical tail  $V_2$ . The increment  $\Delta_1 C_{n_\psi}$  for both configurations varied erratically with angle of attack and indicated no definite trends. The increment  $\Delta_2 C_{n_\psi}$  for the model with the slat was larger (more positive) than for the wing without the slat up to about  $20^\circ$ , after which the opposite was true.

It should be pointed out again that the interference increments presented herein can be expected to apply fairly accurately only to midwing or near-midwing configurations since the height of the wing relative to the fuselage center line has been found to be an important factor in determining interference increments (reference 2).



## CONCLUSIONS

The results of an investigation to determine the effects of vertical-tail size and length and of fuselage shape and length on the lateral static stability characteristics of a model with a  $45^\circ$  sweptback wing indicate the following conclusions:

1. The directional instability of the various isolated fuselages was about two-thirds as large as that predicted by classical theory.

2. A reduction in area (geometric aspect ratio kept constant) of vertical tails attached to a given fuselage resulted in an increase in the effective aspect ratio of the vertical tails for the range of tail sizes considered. Simple analytical considerations indicate, however, that for tail sizes below the range investigated the opposite effect would be expected.

3. For the fuselage-tail combinations investigated, the tail effectiveness usually decreased with increasing angle of attack, with the greatest rate of decrease occurring at angles of attack greater than about  $16^\circ$ .

4. The wing-fuselage interference for the midwing arrangements investigated was only slightly affected by the shape of the fuselage and the interference tended to increase slightly the directional stability of the combinations.

5. The interference effects of the wing tended to decrease the vertical-tail effectiveness, particularly at high angles of attack. The large effects observed were attributed to a partially stalled condition of the wing.

Langley Aeronautical Laboratory  
National Advisory Committee for Aeronautics  
Langley Air Force Base, Va., June 5, 1950

## REFERENCES

1. Jacobs, Eastman N., and Ward, Kenneth E.: Interference of Wing and Fuselage from Tests of 209 Combinations in the N.A.C.A. Variable-Density Tunnel. NACA Rep. 540, 1935.
2. House, Rufus O., and Wallace, Arthur R.: Wind-Tunnel Investigation of Effect of Interference on Lateral-Stability Characteristics of Four NACA 23012 Wings, an Elliptical and a Circular Fuselage, and Vertical Fins. NACA Rep. 705, 1941.
3. Brewer, Jack D., and Lichtenstein, Jacob H.: Effect of Horizontal Tail on Low-Speed Static Lateral Stability Characteristics of a Model Having  $45^\circ$  Sweptback Wing and Tail Surfaces. NACA TN 2010, 1950.
4. Bamber, Millard J.: Effect of Some Present-Day Airplane Design Trends on Requirements for Lateral Stability. NACA TN 814, 1941.
5. DeYoung, John: Theoretical Additional Span Loading Characteristics of Wings with Arbitrary Sweep, Aspect Ratio, and Taper Ratio. NACA TN 1491, 1947.
6. Goodman, Alex, and Fisher, Lewis R.: Investigation at Low Speeds of the Effect of Aspect Ratio and Sweep on Rolling Stability Derivatives of Untapered Wings. NACA Rep. 968, 1950.
7. Munk, Max M.: The Aerodynamic Forces on Airship Hulls. NACA Rep. 184, 1924.

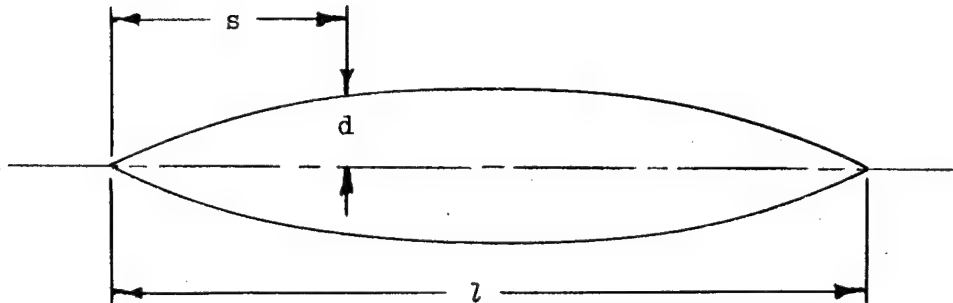
TABLE I.— COORDINATES FOR NACA 65A008 AIRFOIL

[Station and ordinates in percent airfoil chord]

Station	Ordinate
0	0
.50	.62
.75	.75
1.25	.95
2.50	1.30
5.0	1.75
7.5	2.12
10.0	2.43
15	2.93
20	3.30
25	3.59
30	3.79
35	3.93
40	4.00
45	3.99
50	3.90
55	3.71
60	3.46
65	3.14
70	2.76
75	2.35
80	1.90
85	1.43
90	.96
95	.49
100	.02
L. E. radius: 0.408	



TABLE II.- FUSELAGE ORDINATES



$s/l$	$d/l$				
	Fuselage 1	Fuselage 2	Fuselage 3	Fuselage 4	Fuselage 5
0	0	0	0	0	0
.025	.010	.007	.005	.033	.007
.050	.020	.014	.010	.045	.014
.075	.029	.021	.014	.054	.021
.100	.037	.027	.018	.060	.027
.125	.045	.033	.022	.065	.033
.150	.052	.039	.026	.069	.039
.200	.065	.048	.032	.074	.048
.250	.076	.057	.038	.075	.057
.30	.085	.063	.042	.075	.063
.35	.091	.068	.046	.075	.068
.40	.096	.072	.048	.075	.072
.45	.099	.074	.049	.075	.074
.50	.100	.075	.050	.075	.075
.55	.099	.074	.049	.074	.075
.60	.096	.072	.048	.072	.073
.65	.091	.068	.046	.068	.072
.70	.085	.063	.042	.063	.069
.75	.076	.057	.038	.057	.066
.80	.065	.048	.032	.048	.062
.85	.052	.039	.026	.039	.057
.90	.037	.027	.018	.027	.051
.95	.020	.014	.010	.014	.045
1.00	0	0	0	0	.038

TABLE III.- PERTINENT GEOMETRIC CHARACTERISTICS OF MODEL

## Wing:

Aspect ratio, $A_W$ , . . . . .	4.0
Taper ratio, $\lambda_W$ , . . . . .	0.6
Quarter-chord sweep angle, $\Lambda_W$ , deg . . . . .	45
Dihedral angle, deg . . . . .	0
Twist, deg . . . . .	0
NACA airfoil section . . . . .	65A008
Area, $S_W$ , sq ft . . . . .	2.25
Span, $b_W$ , ft . . . . .	3.00
Mean aerodynamic chord, $\bar{c}_W$ , ft . . . . .	0.765

## Fuselage:

	$F_1$	$F_2$	$F_3$	$F_4$	$F_5$
Length, ft . . . . .	2.50	3.34	5.00	3.34	3.34
Fineness ratio . . . . .	5.00	6.67	10.0	6.67	6.67
Volume, $V_F$ , cu ft . . . . .	0.267	0.350	0.526	0.448	0.385
Tail length, $l_V$ , ft (all tails) . . . . .	1.04	1.39	2.09	1.39	1.39
Tail-length ratio, $l_V/b_W$ , (all tails) . . . . .	0.347	0.464	0.697	0.464	0.464
Side area, $S_S$ , sq ft . . . . .	0.833	1.11	1.67	1.30	1.25

## Vertical tail:

	$V_1$	$V_2$	$V_3$	$V_4$	$V_5$
Aspect ratio . . . . .	1.0	1.0	1.0	2.0	2.0
Taper ratio . . . . .	0.6	0.6	0.6	0.6	0.6
Quarter-chord sweep angle, $\Lambda_V$ , deg . . . . .	45	45	45	45	45
NACA airfoil section . . . . .	65A008	65A008	65A008	65A008	65A008
Area, $S_V$ , sq ft . . . . .	0.169	0.338	0.506	0.338	0.675
Span, $b_V$ , ft . . . . .	0.408	0.583	0.710	0.825	1.159
Mean aerodynamic chord, $\bar{c}_V$ , ft . . . . .	0.417	0.592	0.725	0.416	0.592
Area ratio, $S_V/S_W$ . . . . .	0.075	0.150	0.225	0.150	0.300



TABLE IV.- CONFIGURATIONS INVESTIGATED

Wing off		Wing on	
Configuration (a)	Figure	Configuration (a)	Figure
-----	-----	W	6,7
$F_1$ $F_1 + V_1$ $F_1 + V_2$ $F_1 + V_3$	8(a)	$W + F_1$ $W + F_1 + V_1$ $W + F_1 + V_2$ $W + F_1 + V_3$	9(a)
$F_2$ $F_2 + V_1$ $F_2 + V_2$ $F_2 + V_3$	8(b),12 8(b) 8(b) 8(b)	$W + F_2$ $W + F_2 + V_1$ $W + F_2 + V_2$ $W + F_2 + V_3$	9(b),13 9(b) 9(b) 9(b)
$F_3$ $F_3 + V_1$ $F_3 + V_2$ $F_3 + V_3$	8(c)	$W + F_3$ $W + F_3 + V_1$ $W + F_3 + V_2$ $W + F_3 + V_3$	9(c)
$F_4$ $F_4 + V_2$	10(a)	$W + F_4$ $W + F_4 + V_2$	10(b)
$F_5$ $F_5 + V_2$	11(a)	$W + F_5$ $W + F_5 + V_2$	11(b)
$F_2 + V_4$ $F_2 + V_5$	12	$W + F_2 + V_4$ $W + F_2 + V_5$	13
-----	-----	$W_S$	6,7,14
-----	-----	$W_S + F_2$	14
-----	-----	$W_S + F_2 + V_2$	14

<sup>a</sup>Notation(for details, see table III and figs. 2 to 4):

W wing; with subscript S, wing with slat

F fuselage

V vertical tail



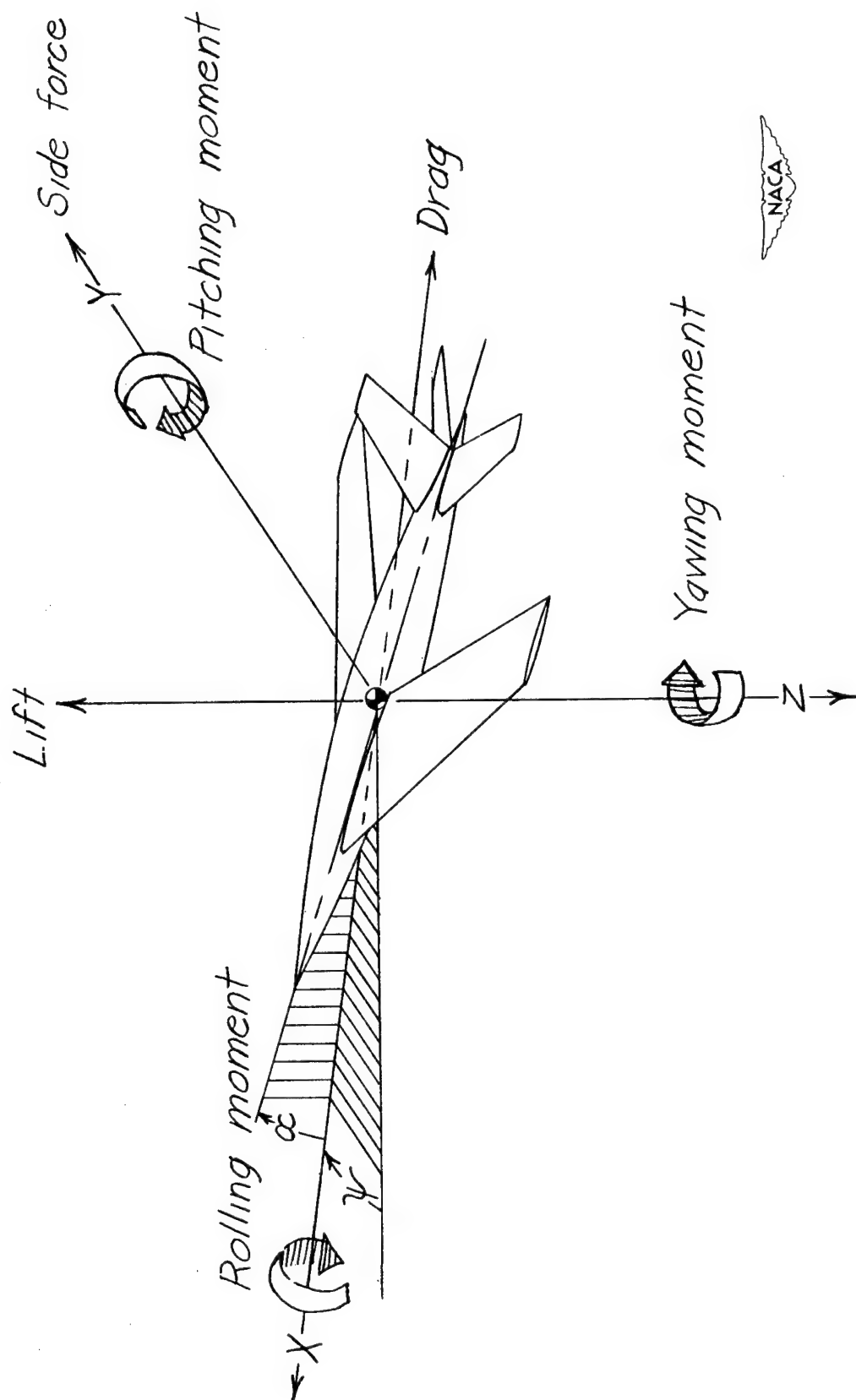


Figure 1.- System of axes used. Arrows indicate positive direction of angles, forces, and moments.

• Location of  $\bar{c}_V/4$

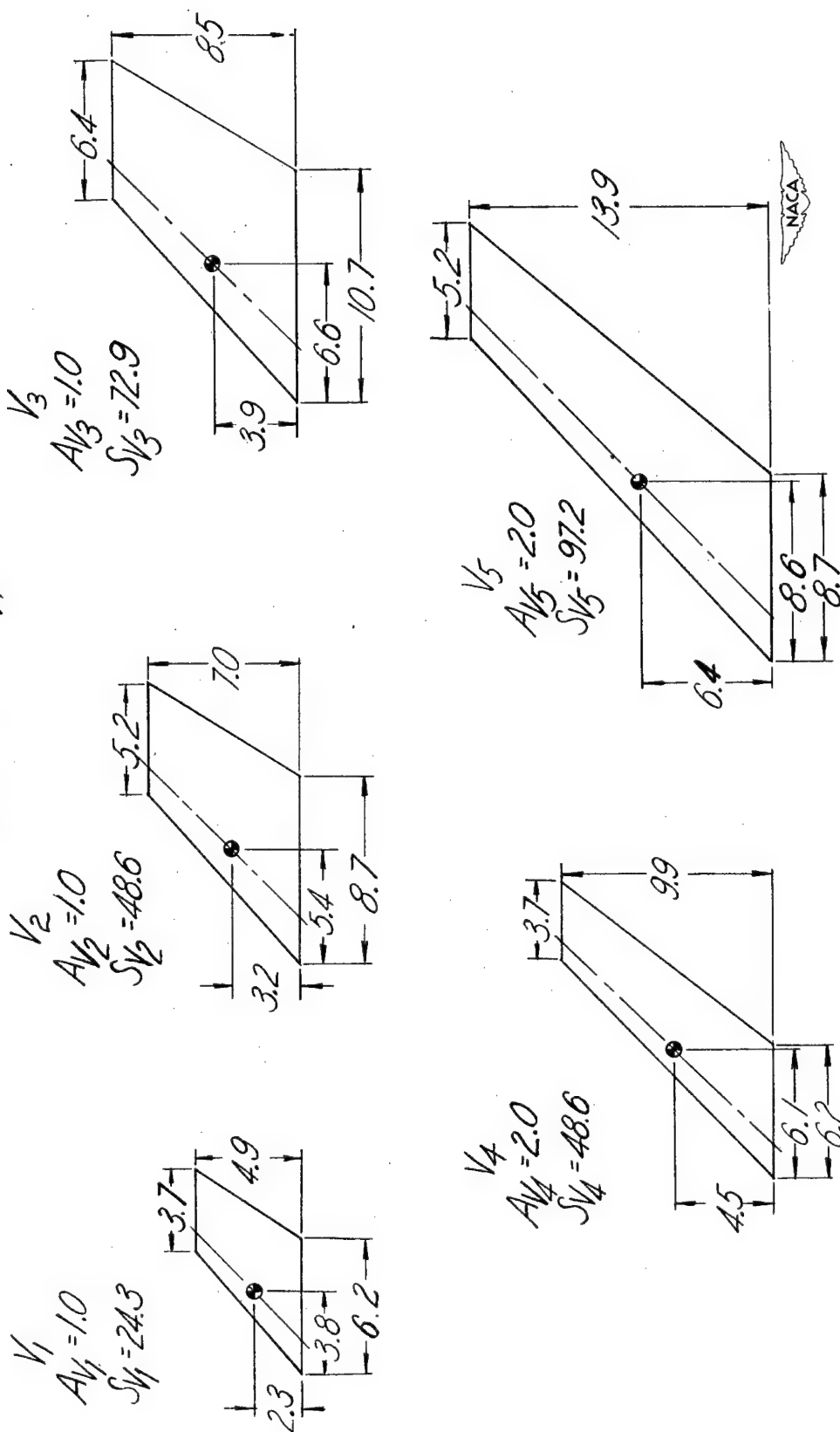


Figure 2.- Dimensions of vertical tails tested.  $\lambda = 0.6$ ;  $\Lambda = 45^\circ$ ; profile, NACA 65A008. All dimensions are in inches.



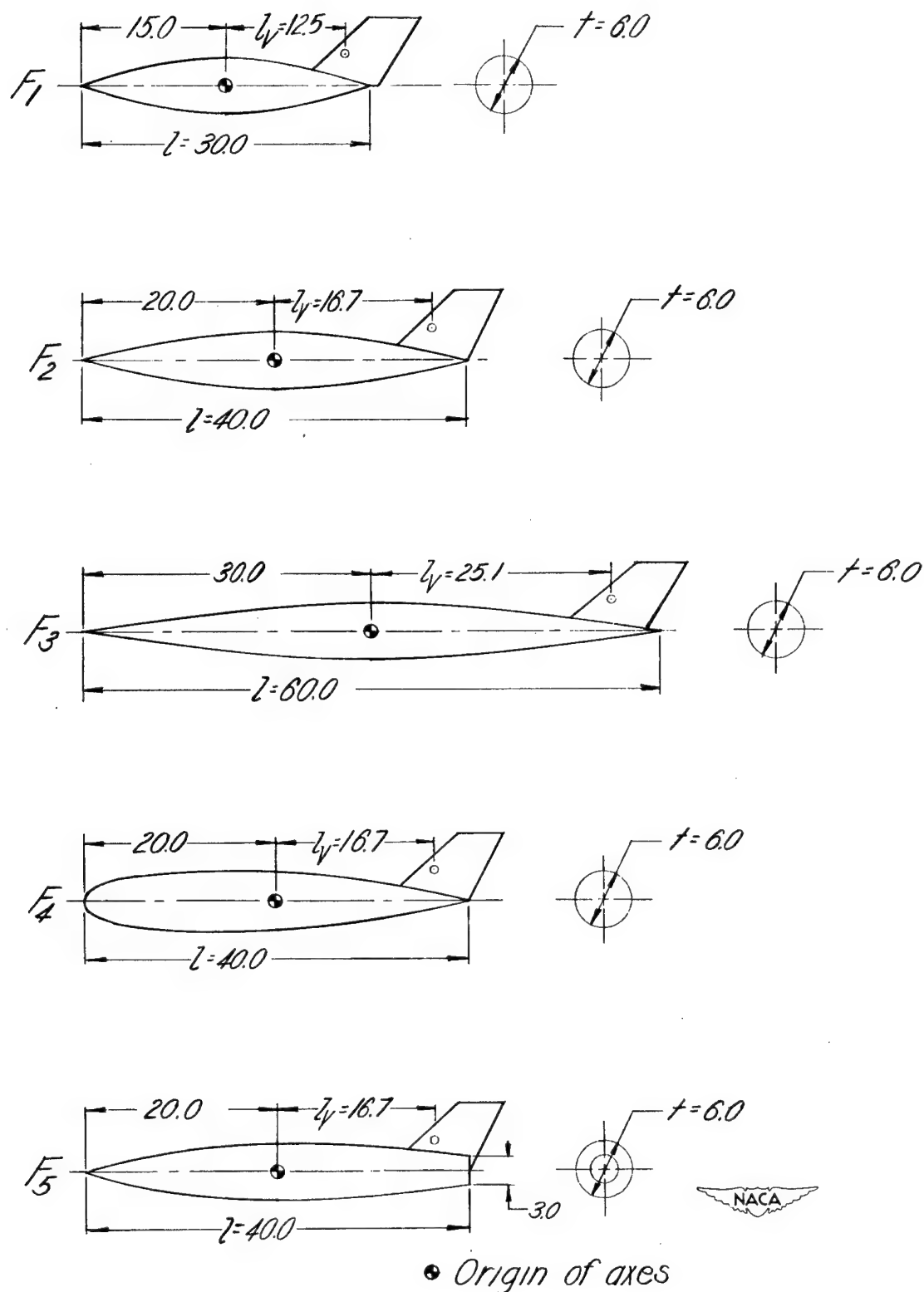


Figure 3.- Dimensions of fuselages; profile ordinates in table II. All dimensions are in inches.

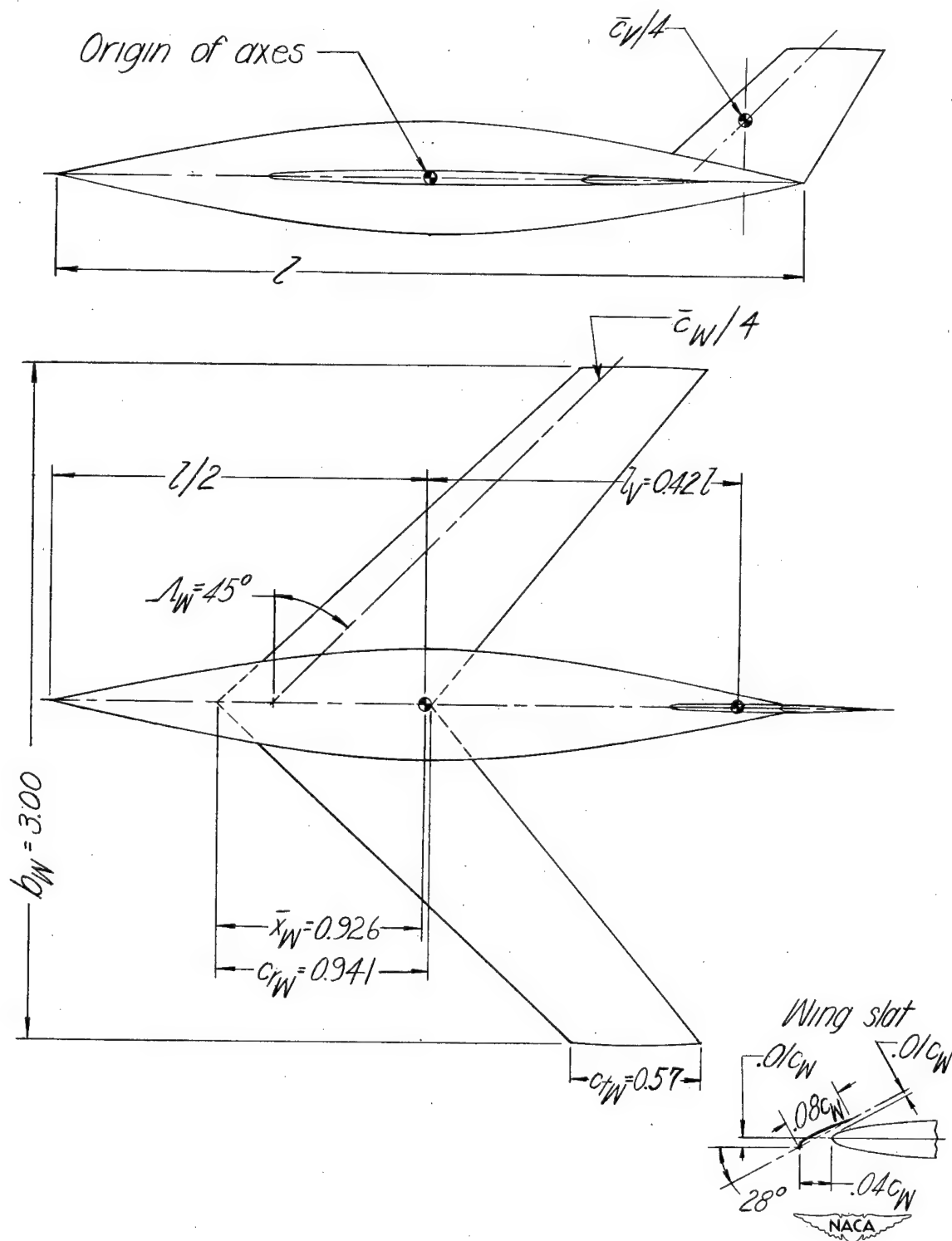
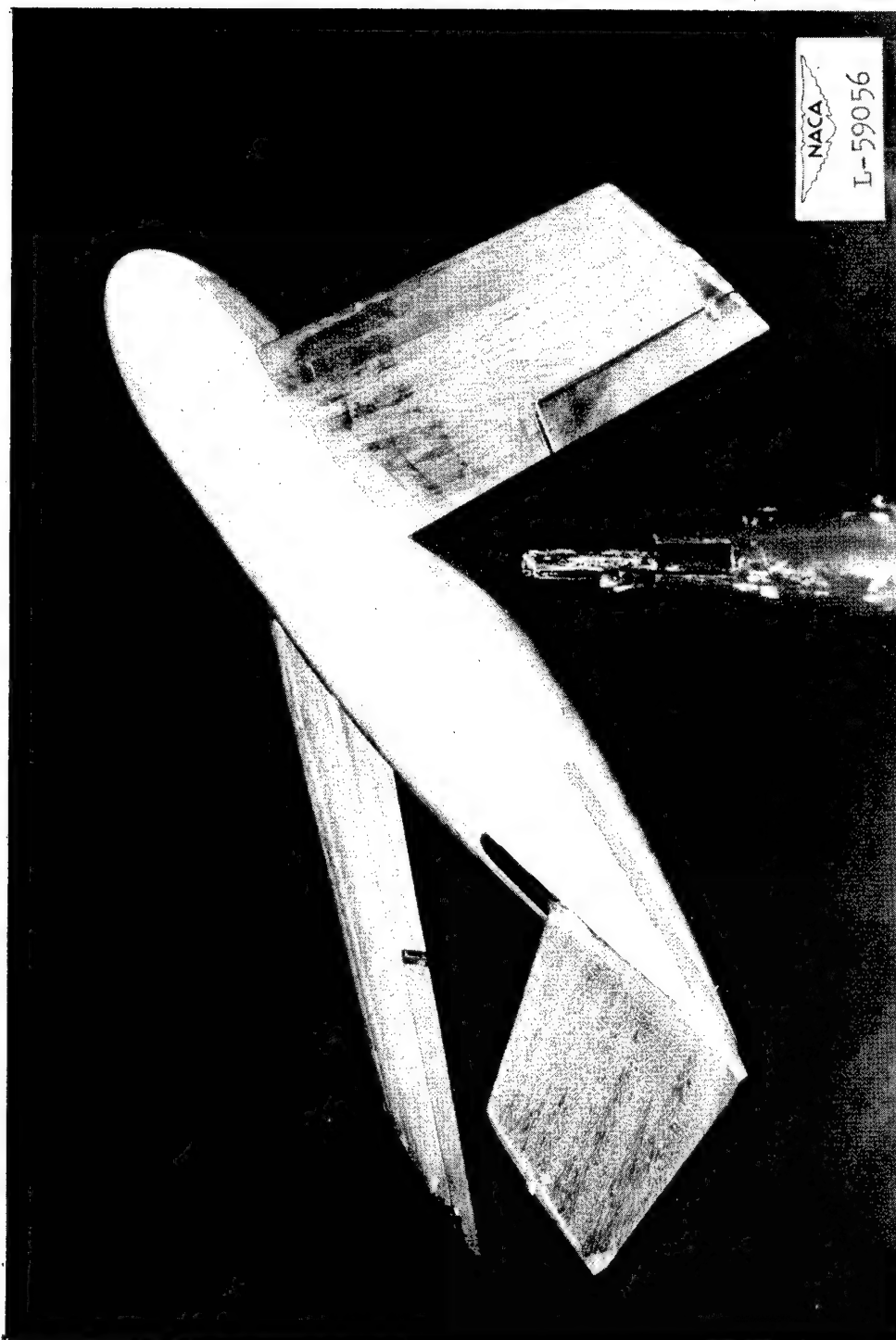
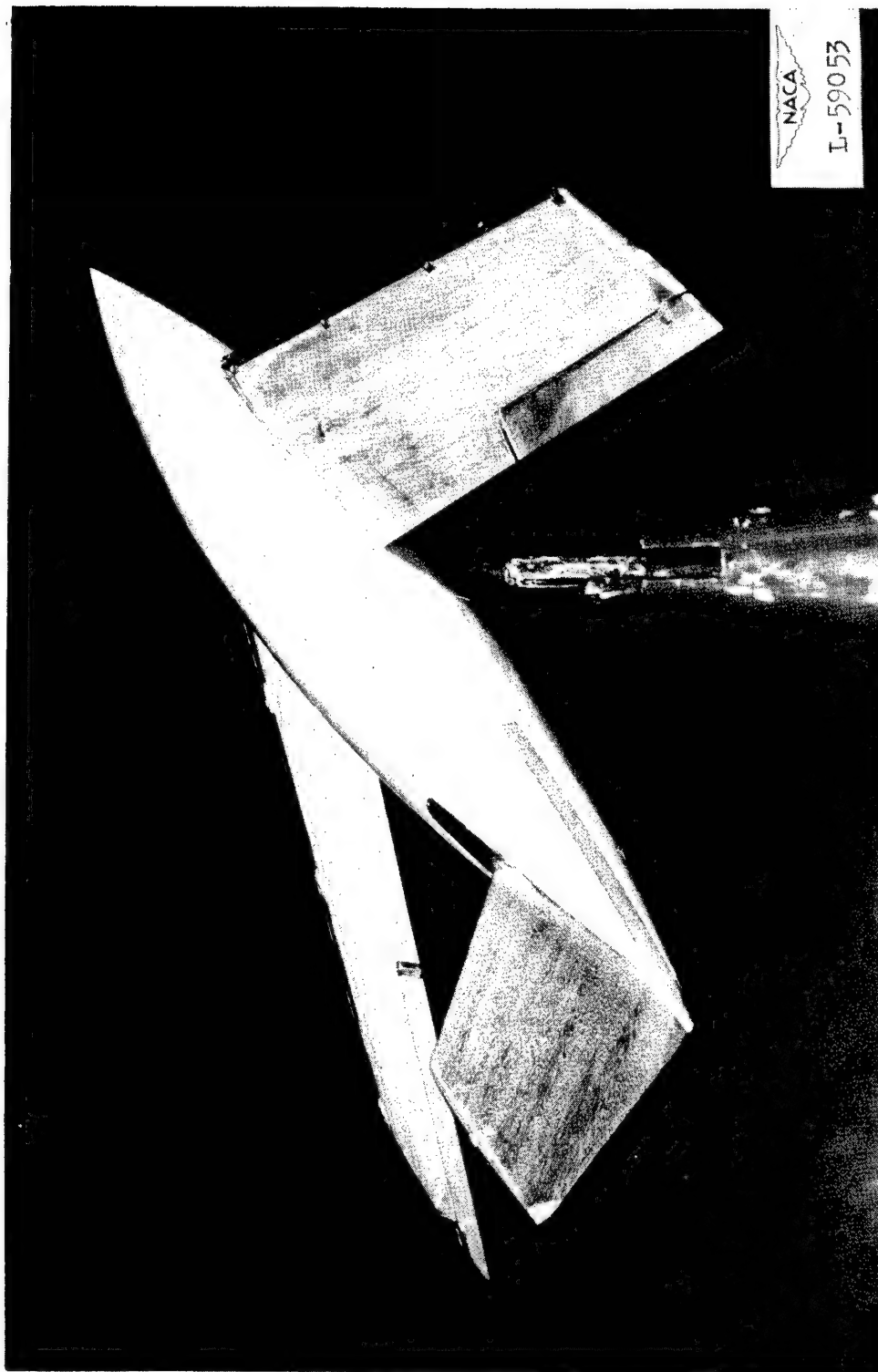


Figure 4.- Dimensions and location of wing and vertical tails. All dimensions are in feet..



(a) Configuration  $W + F_4 + V_2$ .

Figure 5.- View of model in the Langley stability tunnel.



(b) Configuration  $W_S + F_2 + V_2$ .

Figure 5.- Concluded.

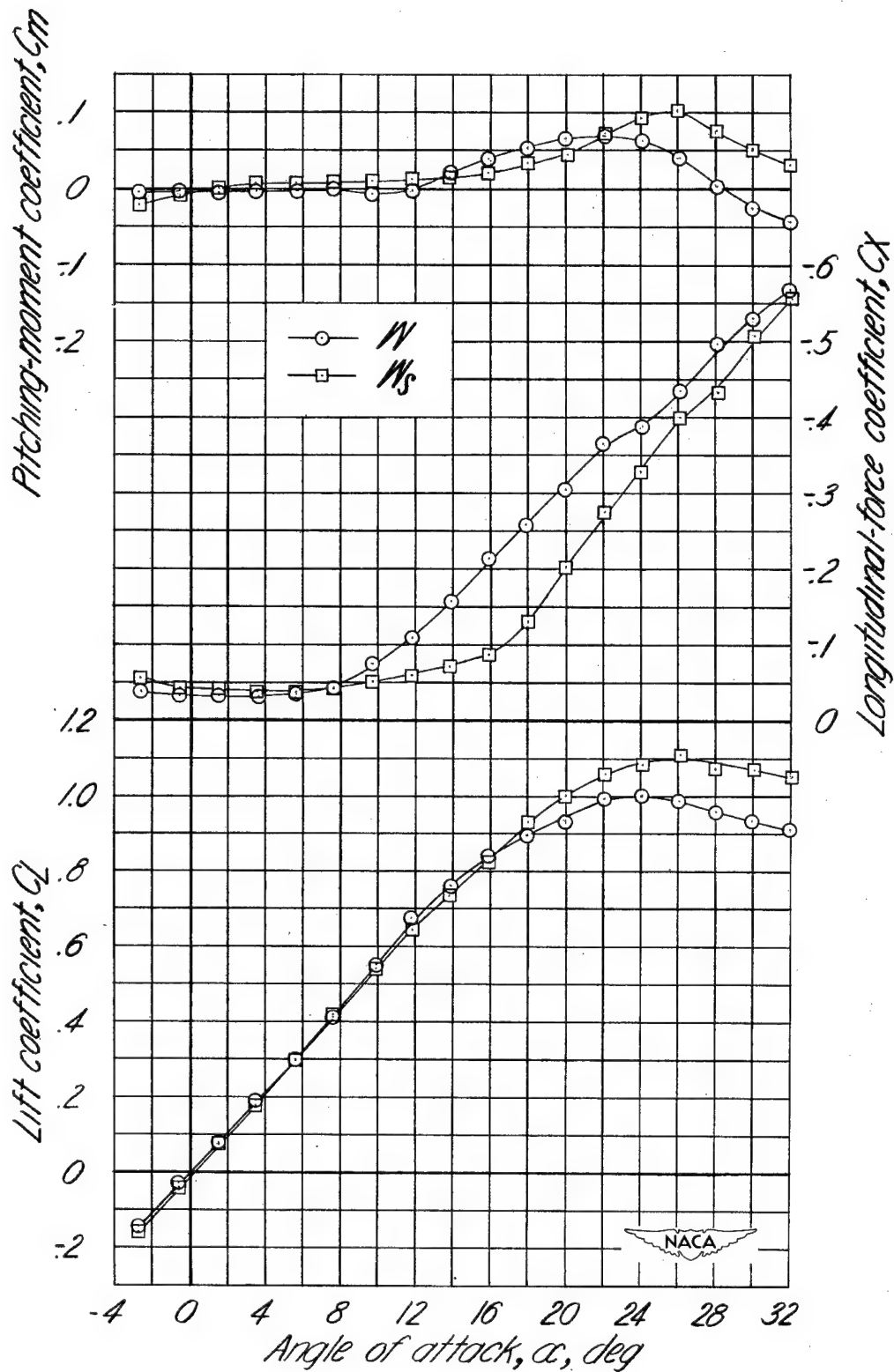


Figure 6.- Aerodynamic characteristics of the wing.

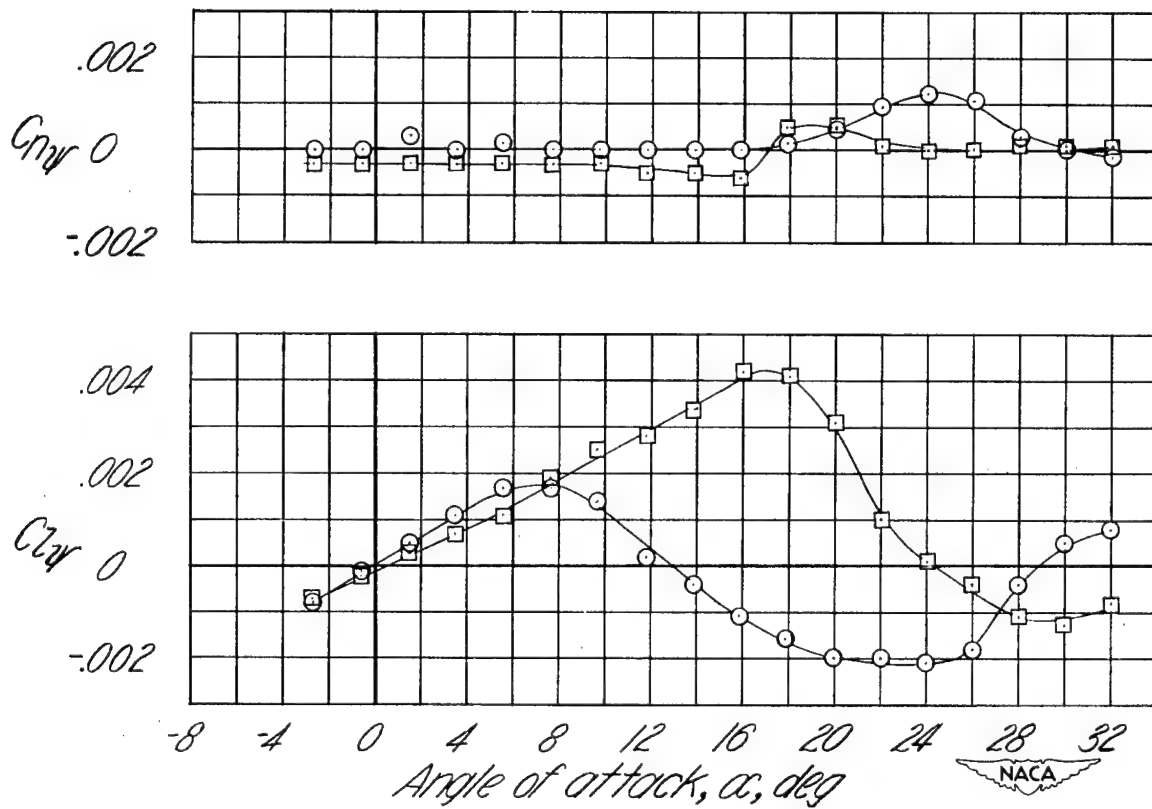
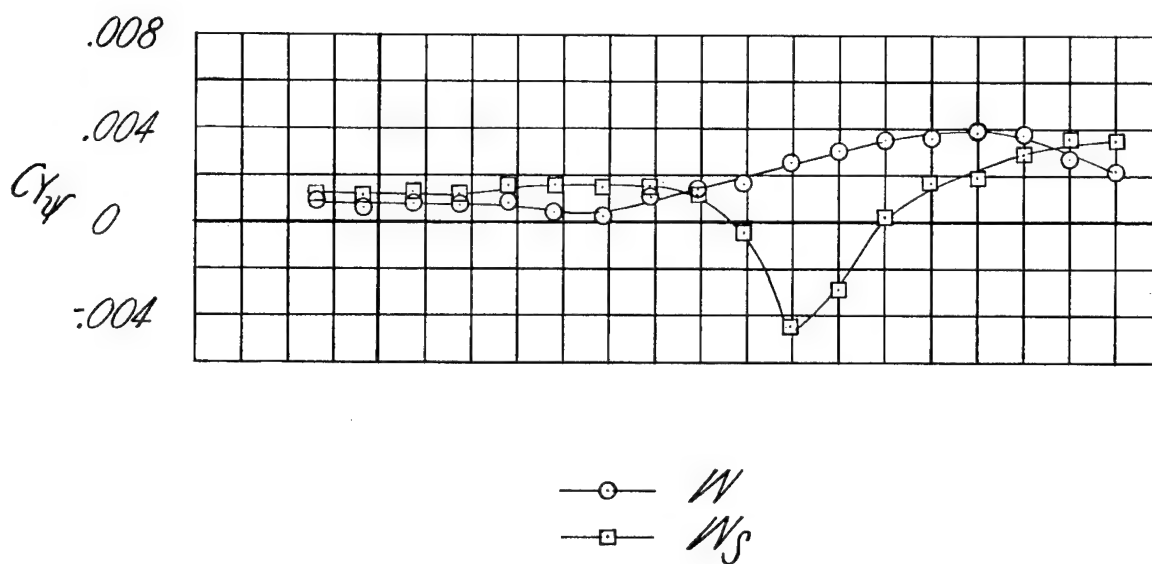
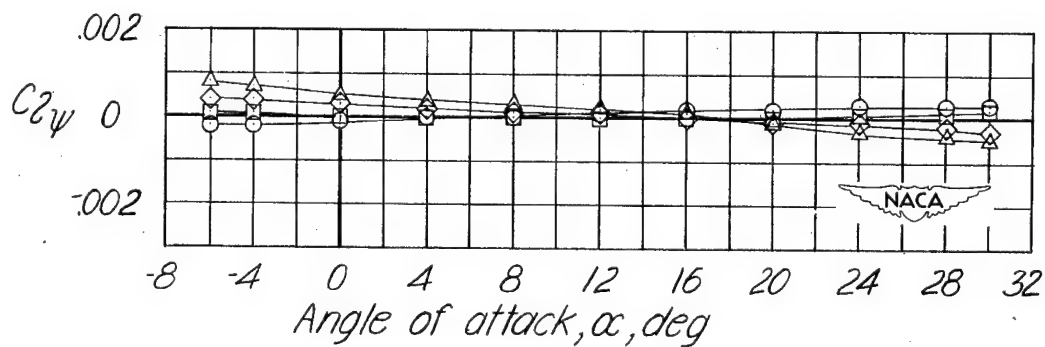
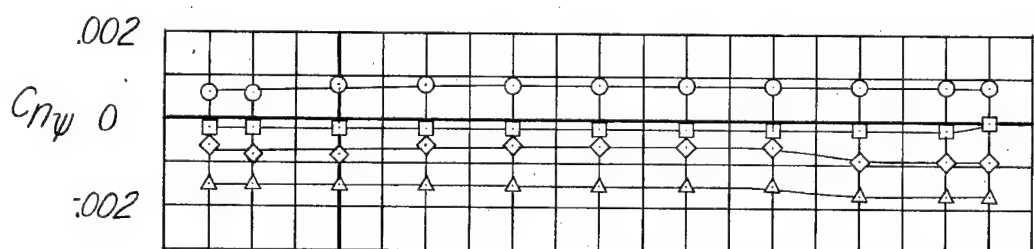
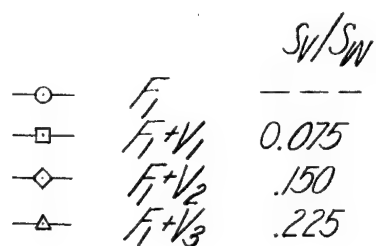
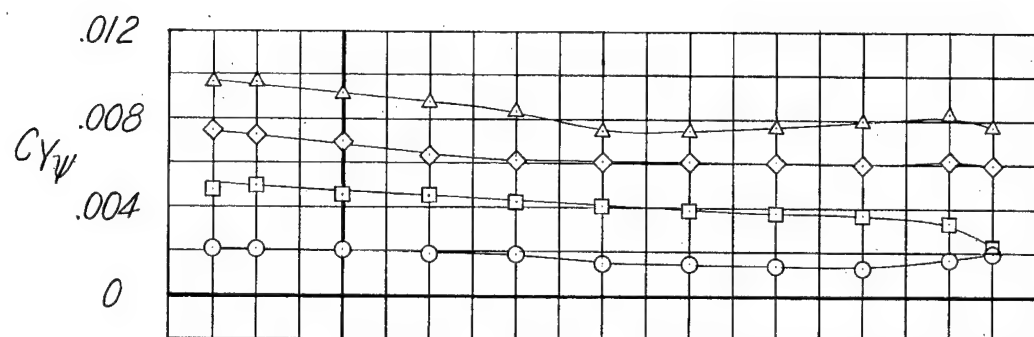
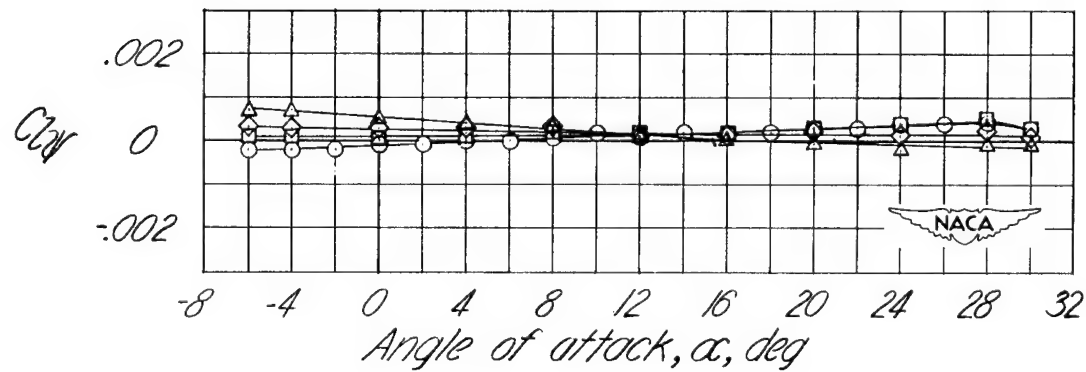
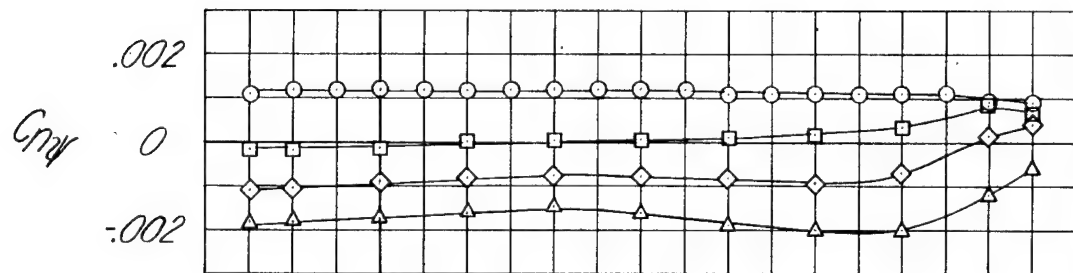
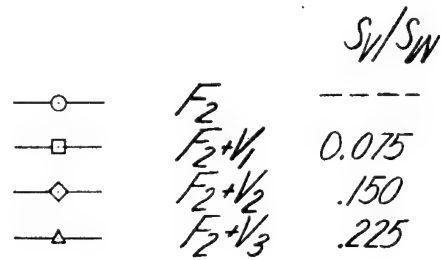
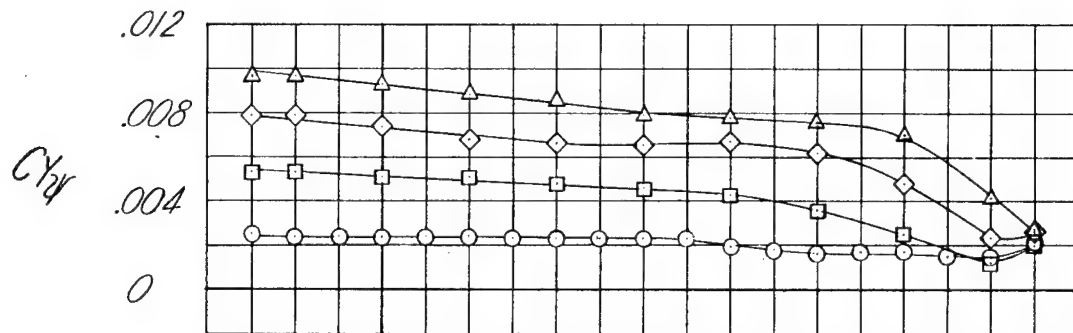


Figure 7.- Static lateral stability characteristics of the wing.



(a) Fuselage 1 (short).

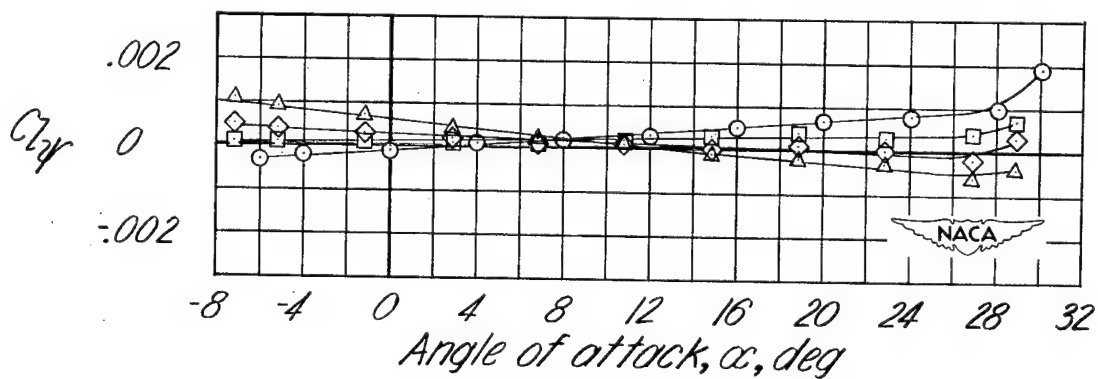
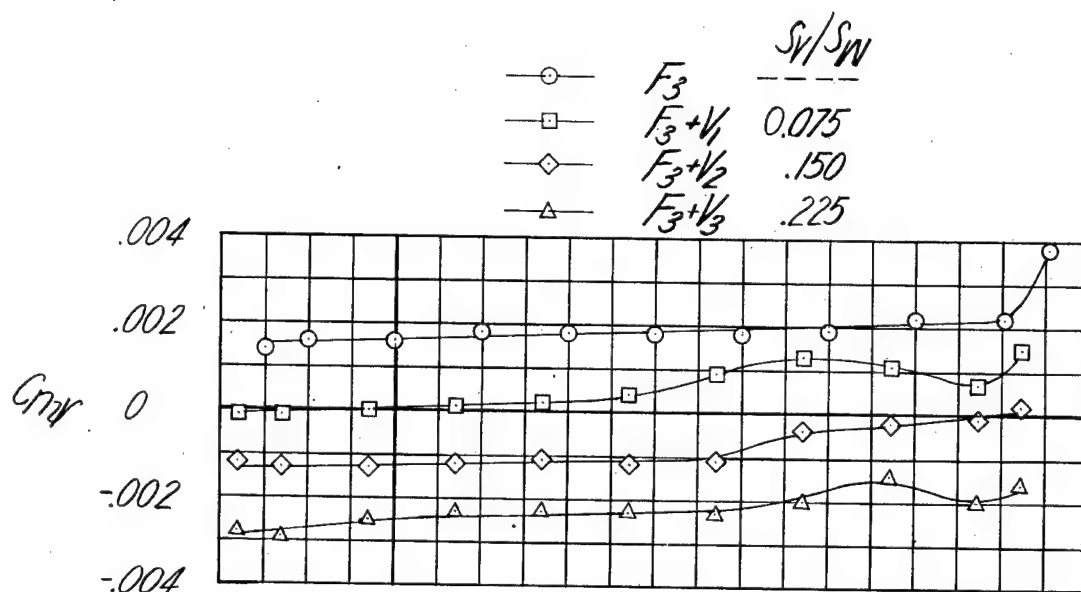
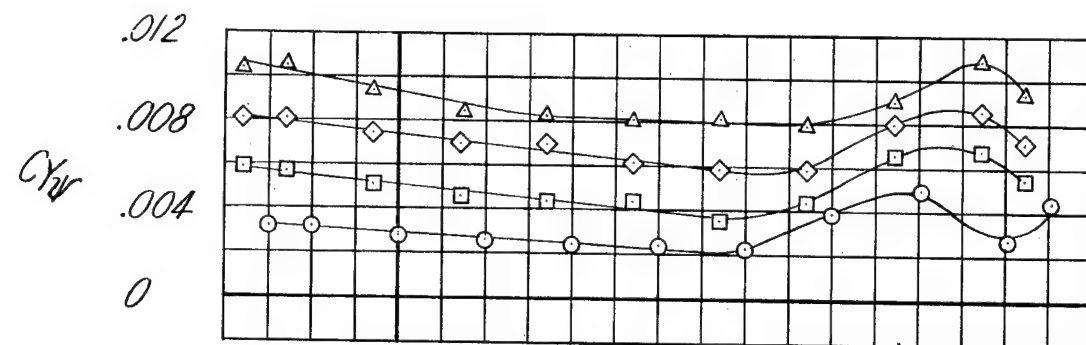
Figure 8.- Effect of vertical tail on the static lateral stability characteristics. Wing off;  $A_v = 1.0$ .



(b) Fuselage 2 (medium).

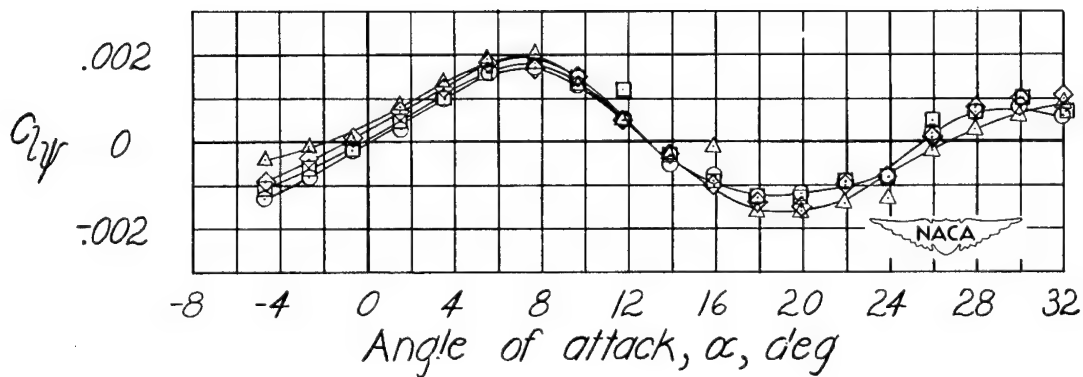
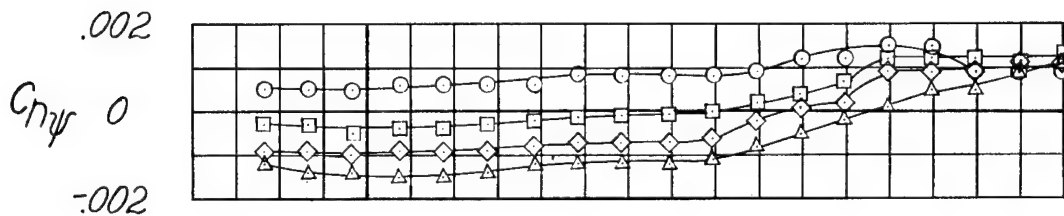
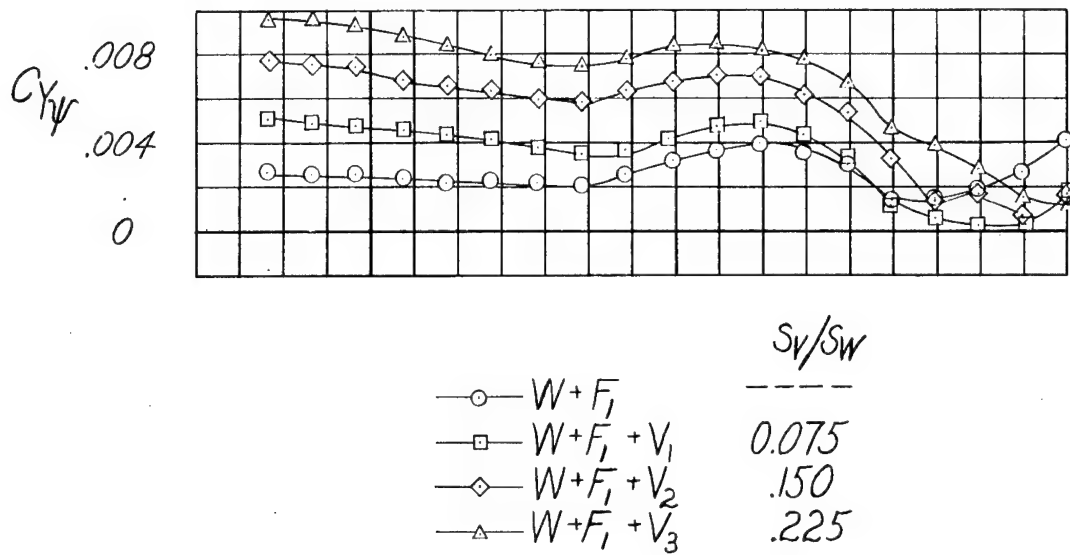
Figure 8.- Continued.





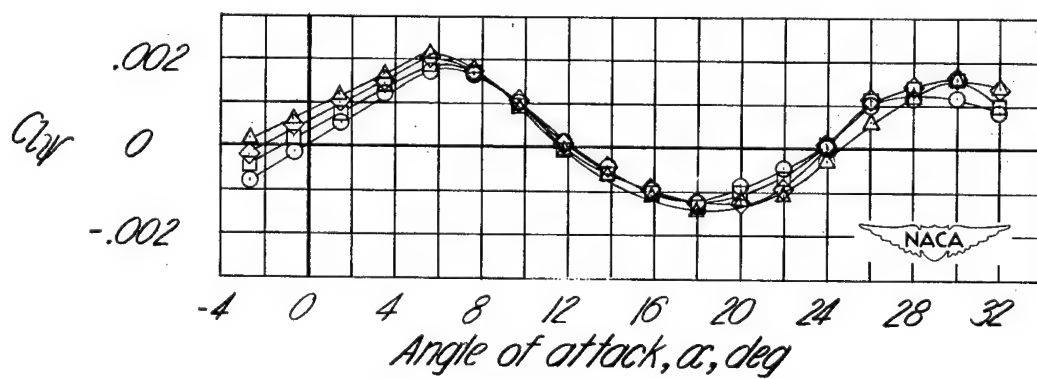
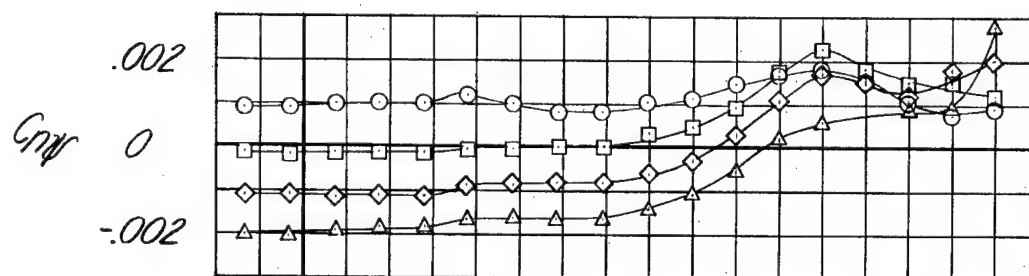
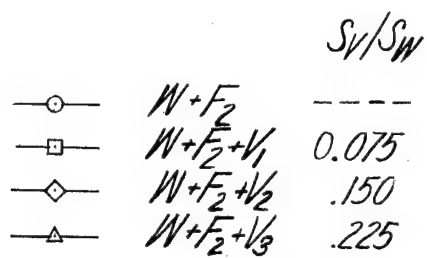
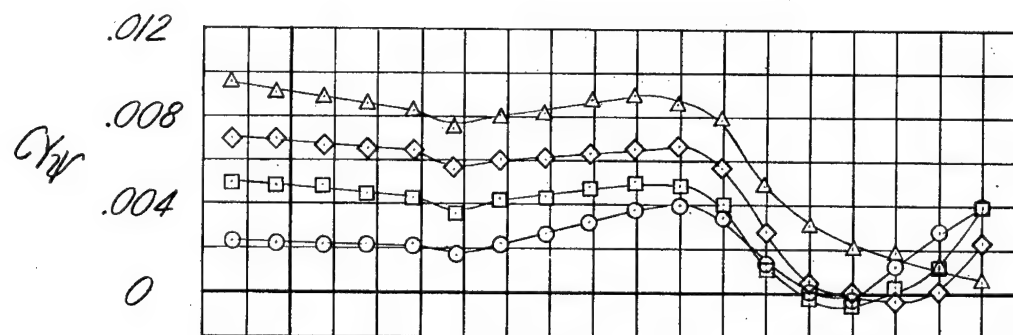
(c) Fuselage 3 (long).

Figure 8.- Concluded.



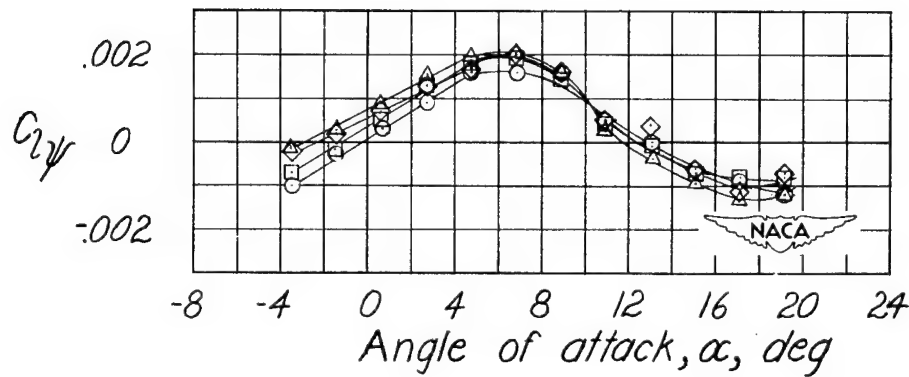
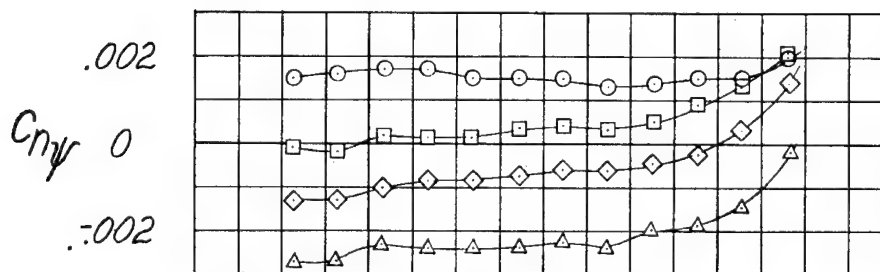
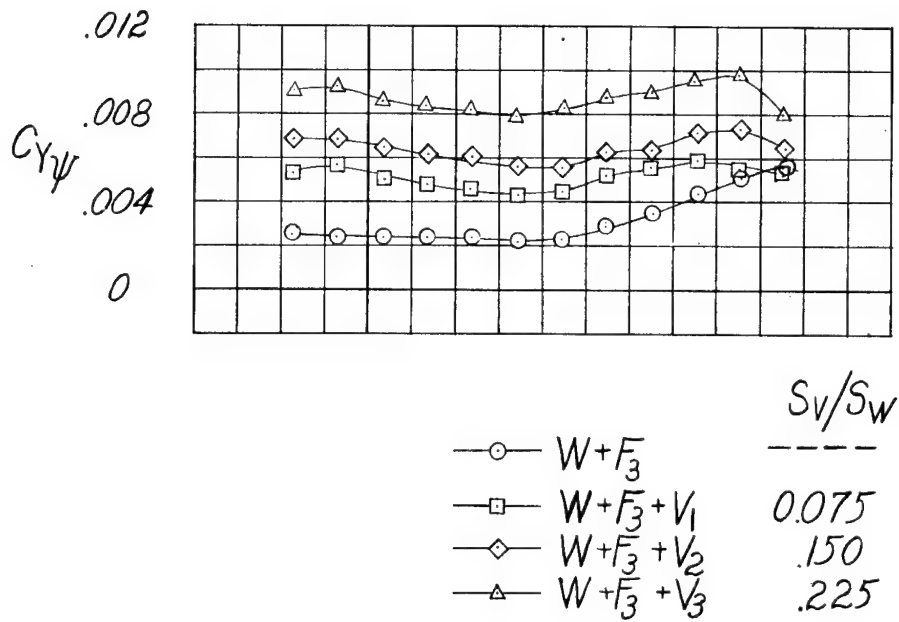
(a) Fuselage 1 (short).

Figure 9.- Effect of vertical tail on the static lateral stability characteristics. Wing on;  $A_V = 1.0$ .



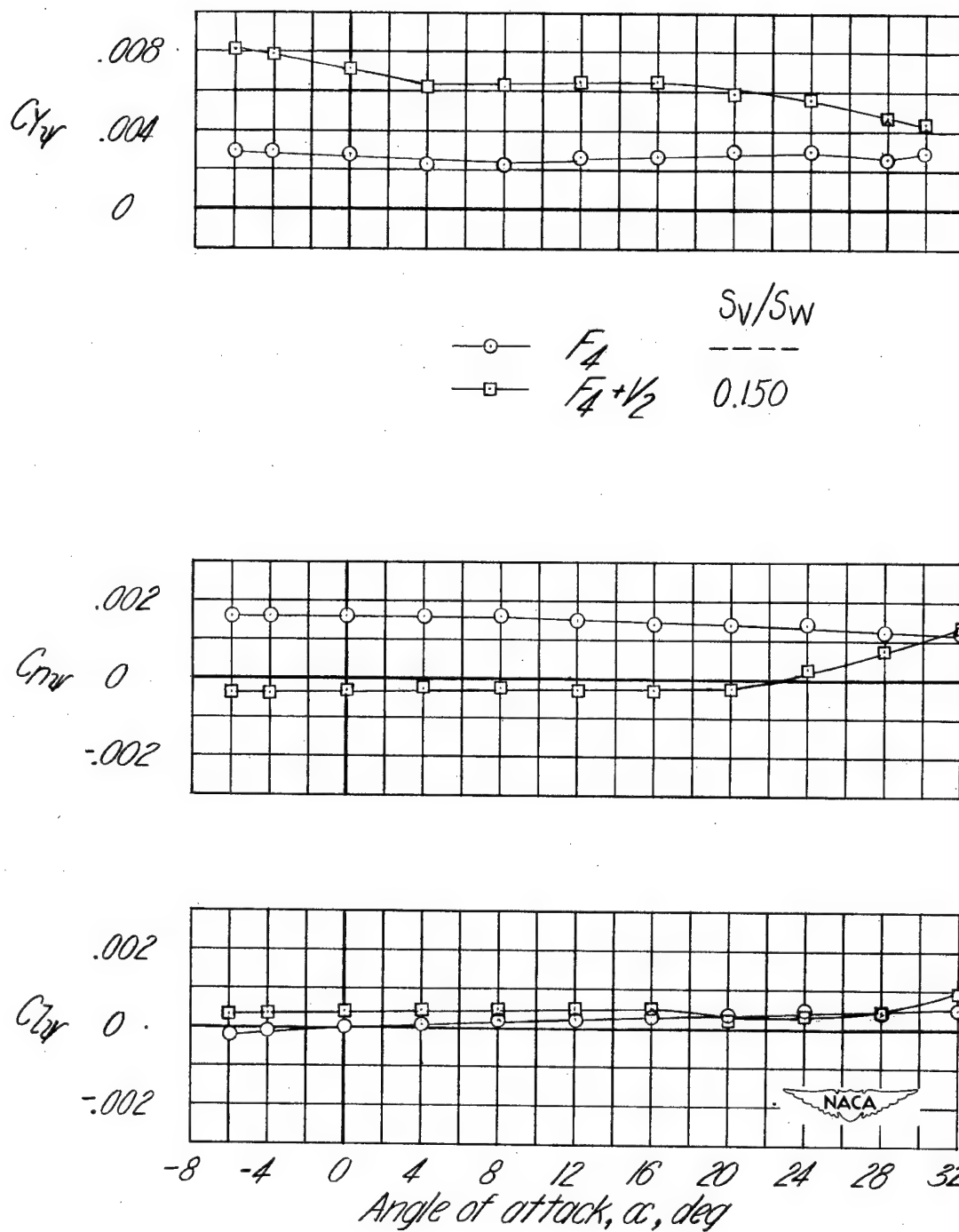
(b) Fuselage 2 (medium).

Figure 9.- Continued.



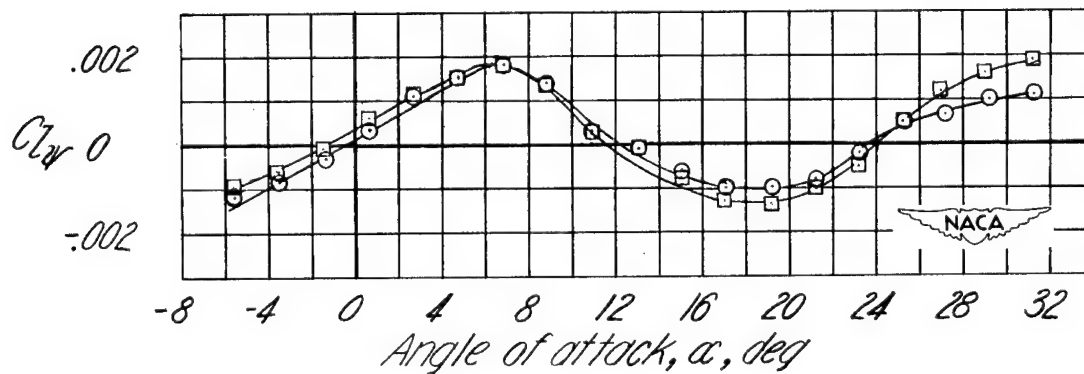
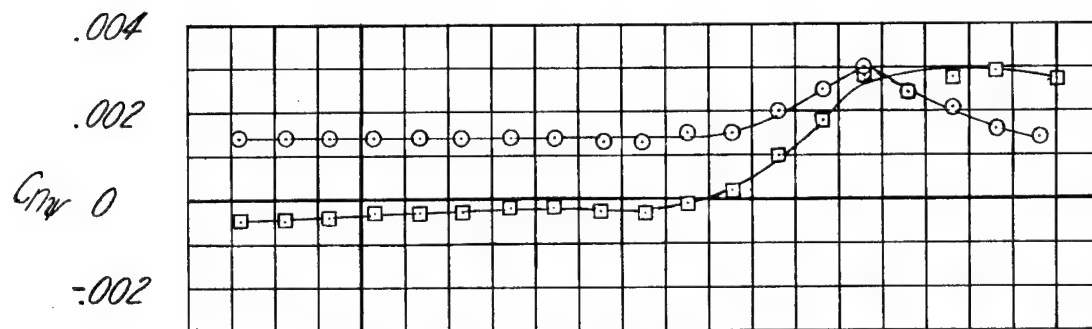
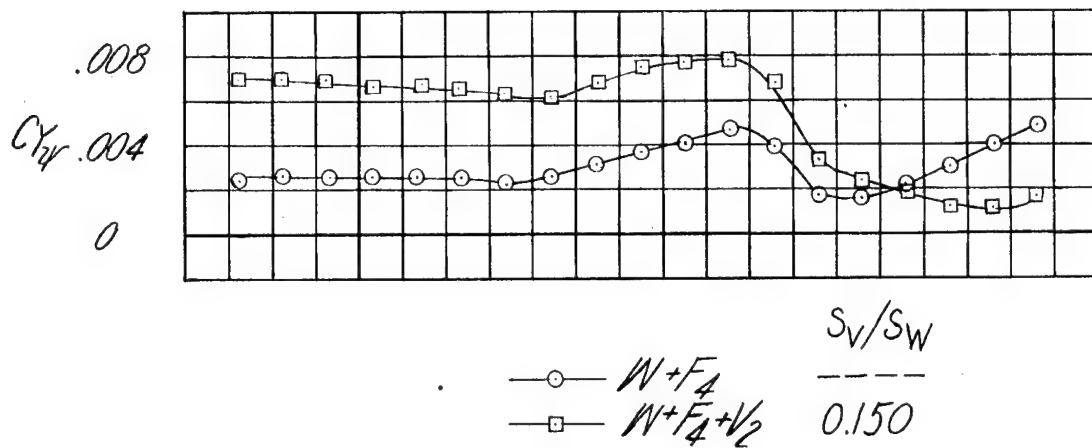
(c) Fuselage 3 (long).

Figure 9.- Concluded.



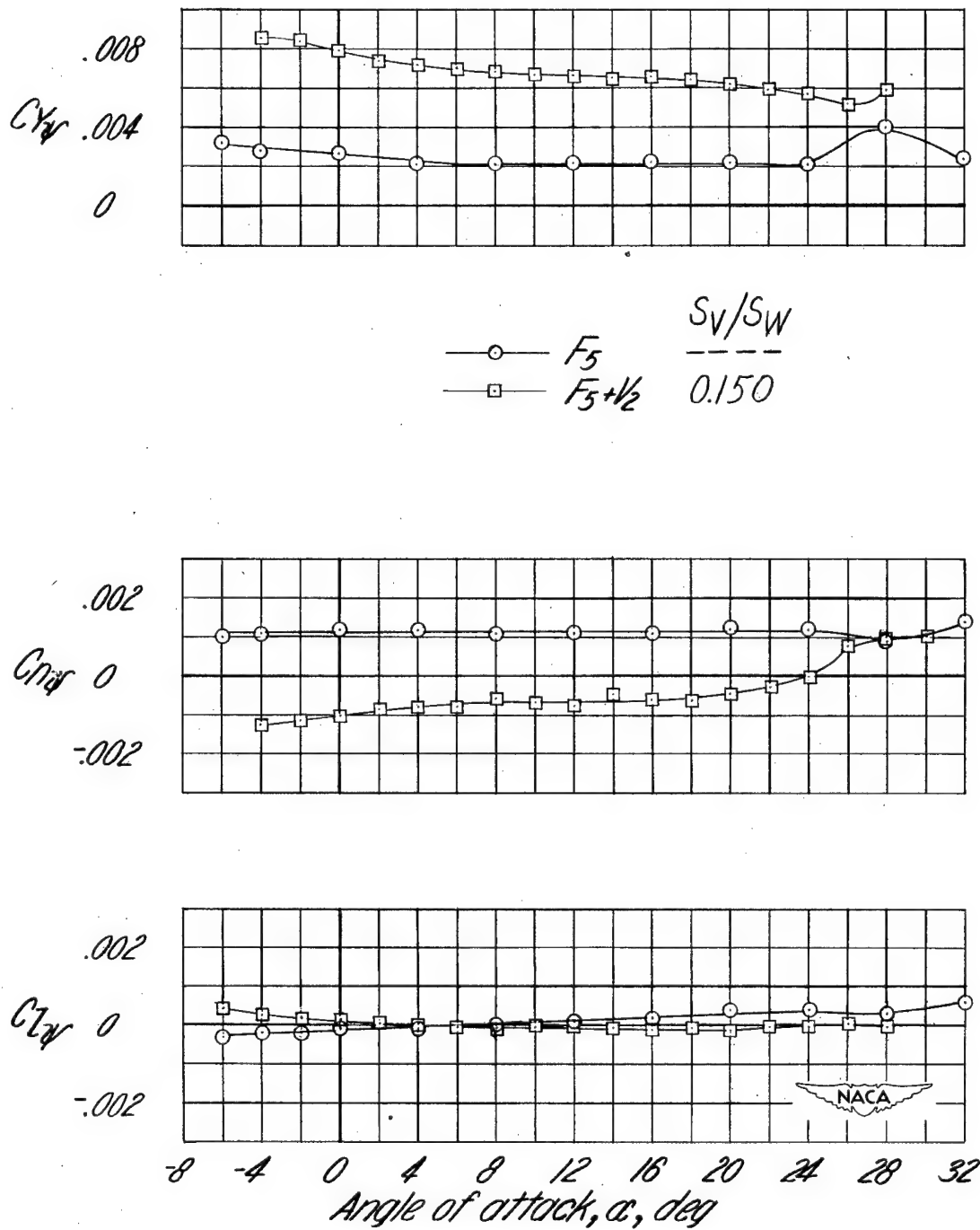
(a) Wing off.

Figure 10.- Static lateral stability characteristics obtained with the blunt-nose fuselage.  $A_v = 1.0$ .



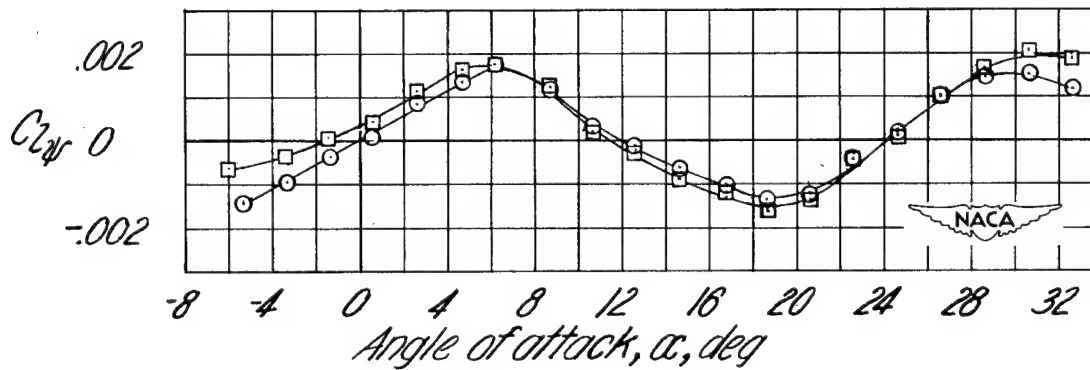
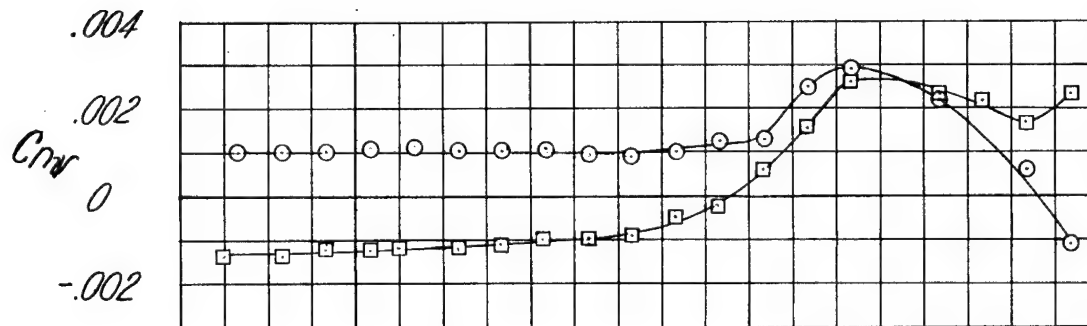
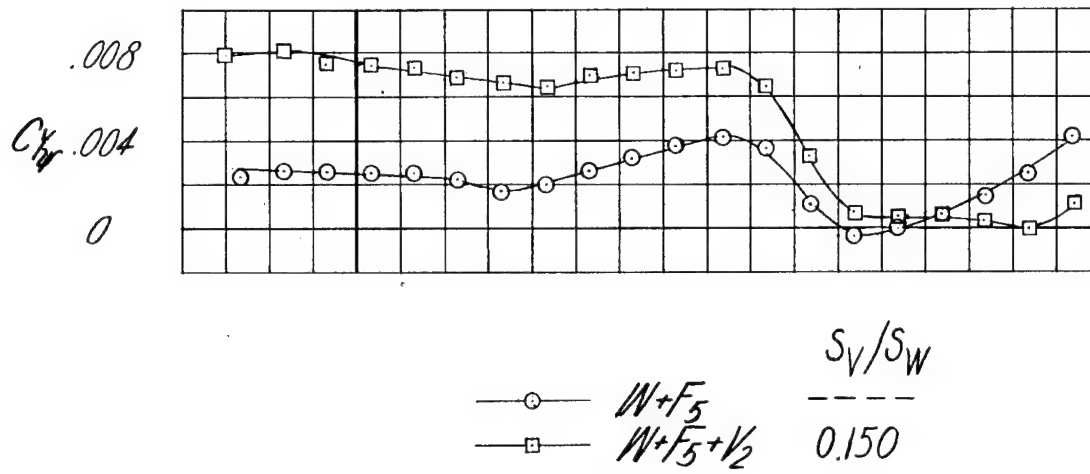
(b) Wing on.

Figure 10.- Concluded.



(a) Wing off.

Figure 11.- Static lateral stability characteristics obtained with blunt-end fuselage.  $A_V = 1.0$ .



(b) Wing on.

Figure 11.- Concluded.



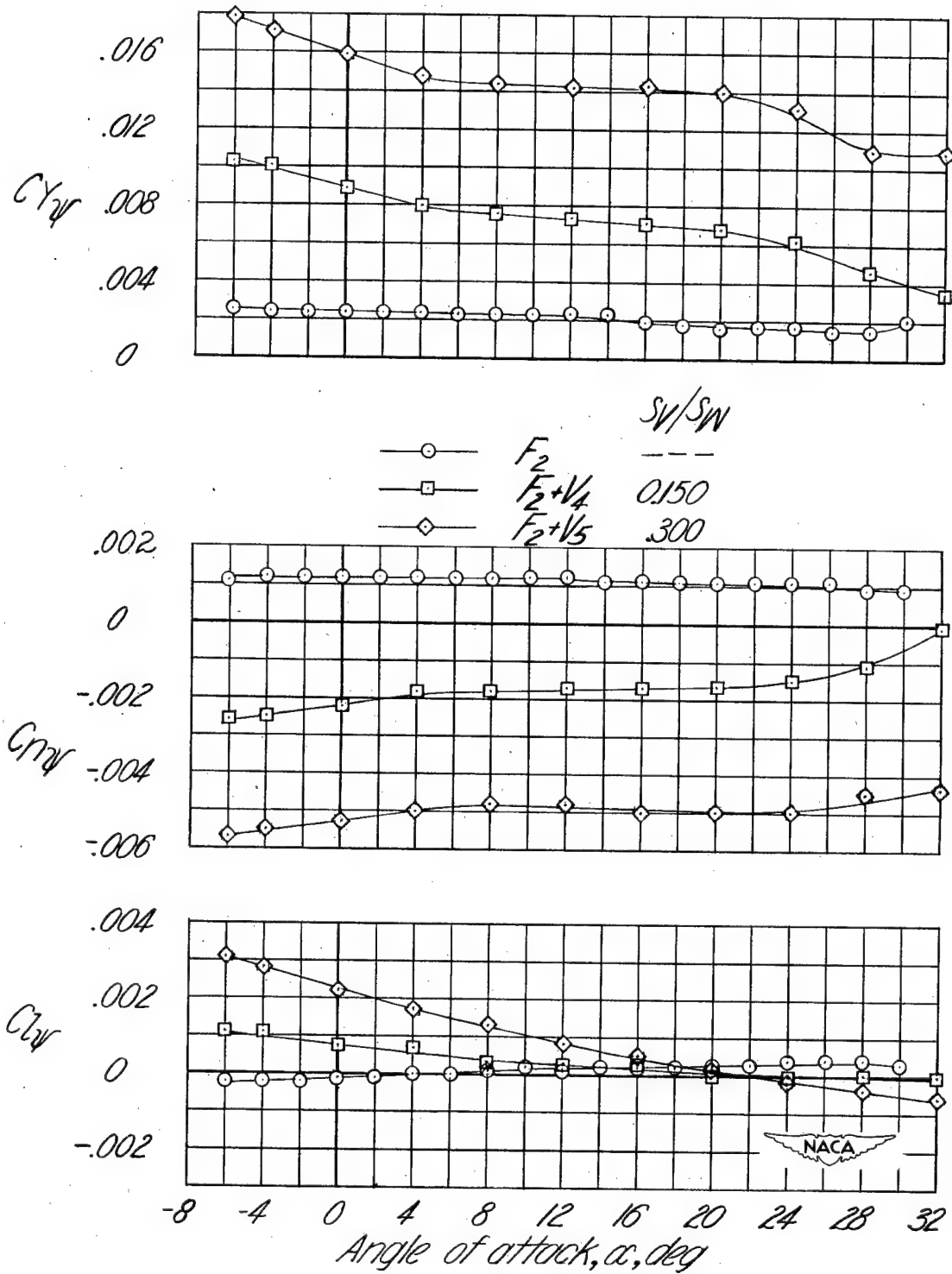


Figure 12.- Effect of vertical tail on the static lateral stability characteristics. Wing off; fuselage 2;  $A_v = 2.0$ .

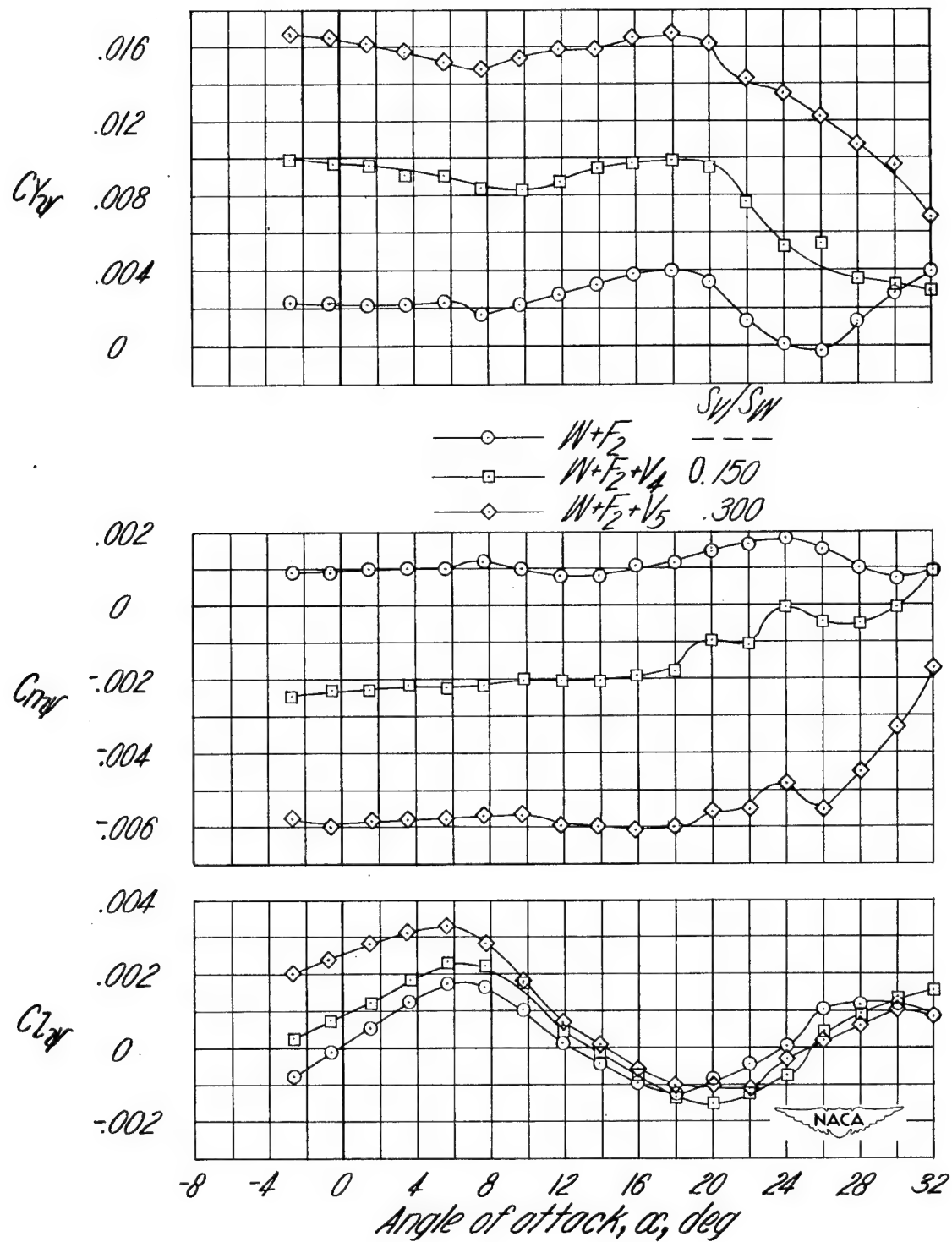


Figure 13.- Effect of vertical tail on the static lateral stability characteristics. Wing on; fuselage 2;  $A_v = 2.0$ .

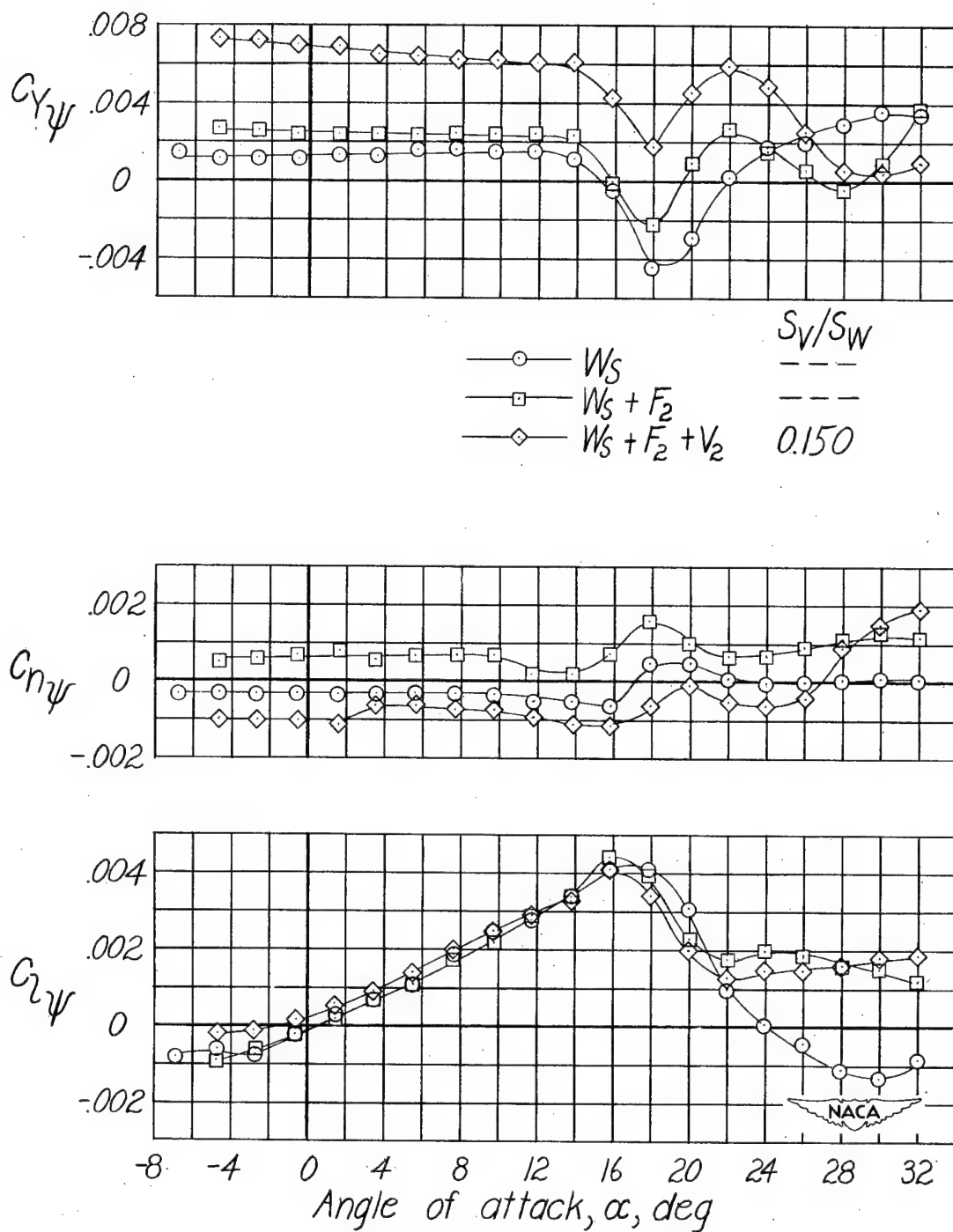


Figure 14.- Static lateral stability characteristics of configurations having wing leading-edge slat.  $A_V = 1.0$ .

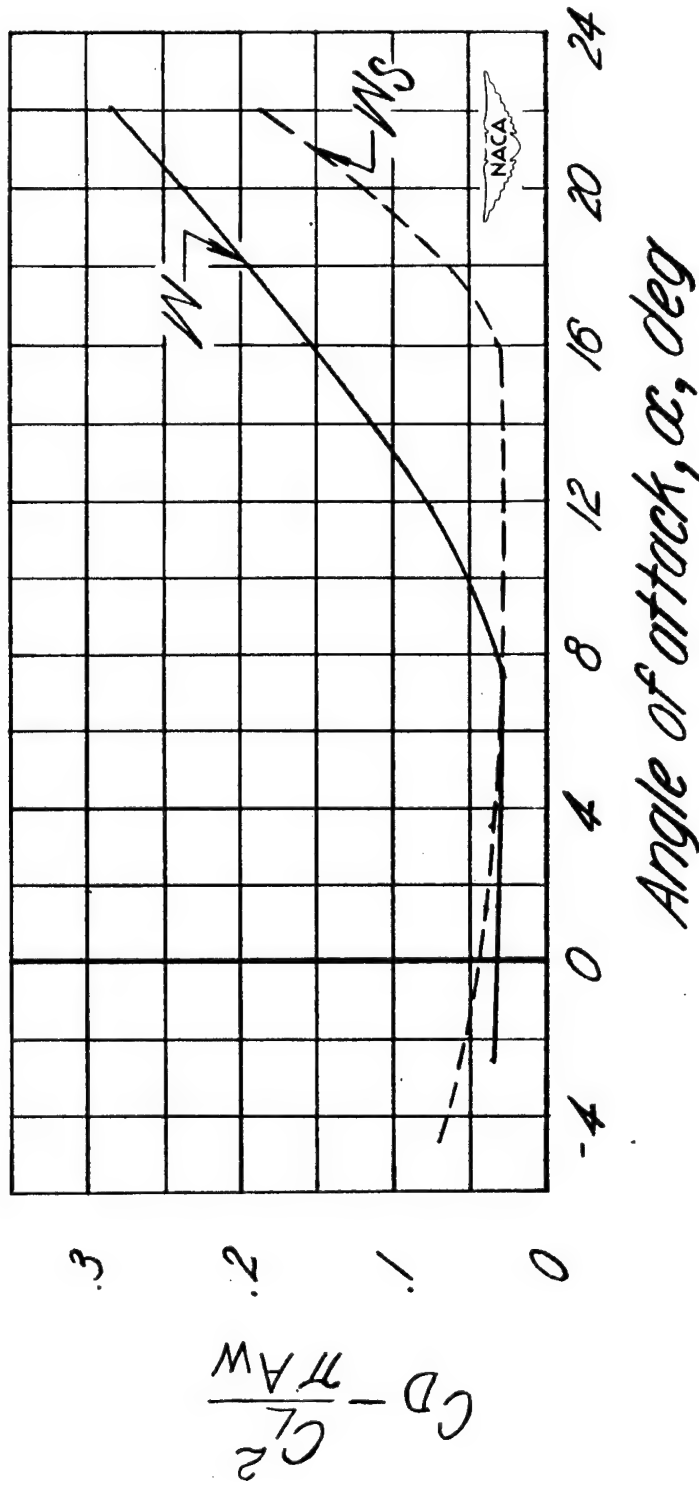
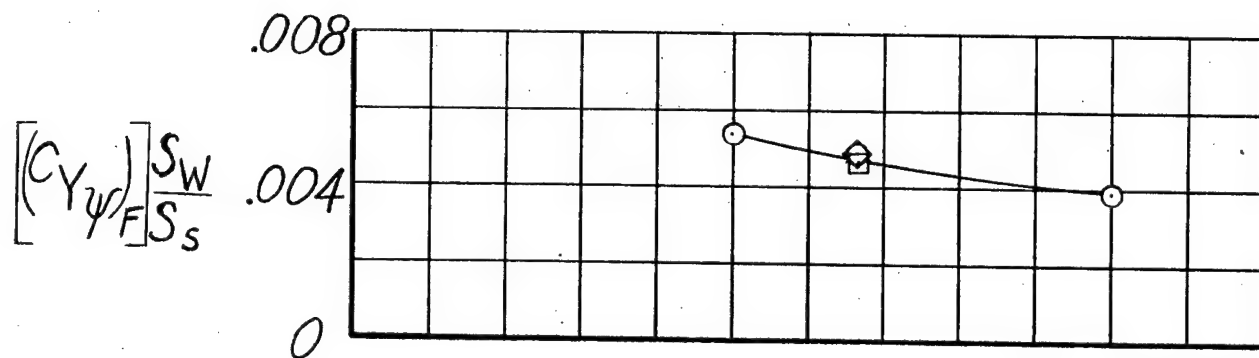


Figure 15.- Effect of wing leading-edge slat on the variation of  $C_D - \frac{C_L^2}{\pi A_W}$  of the wing with angle of attack.



Fuselage  
 ○ 1, 2, 3  
 □ 4  
 ◇ 5  
 --- Theory of reference 7

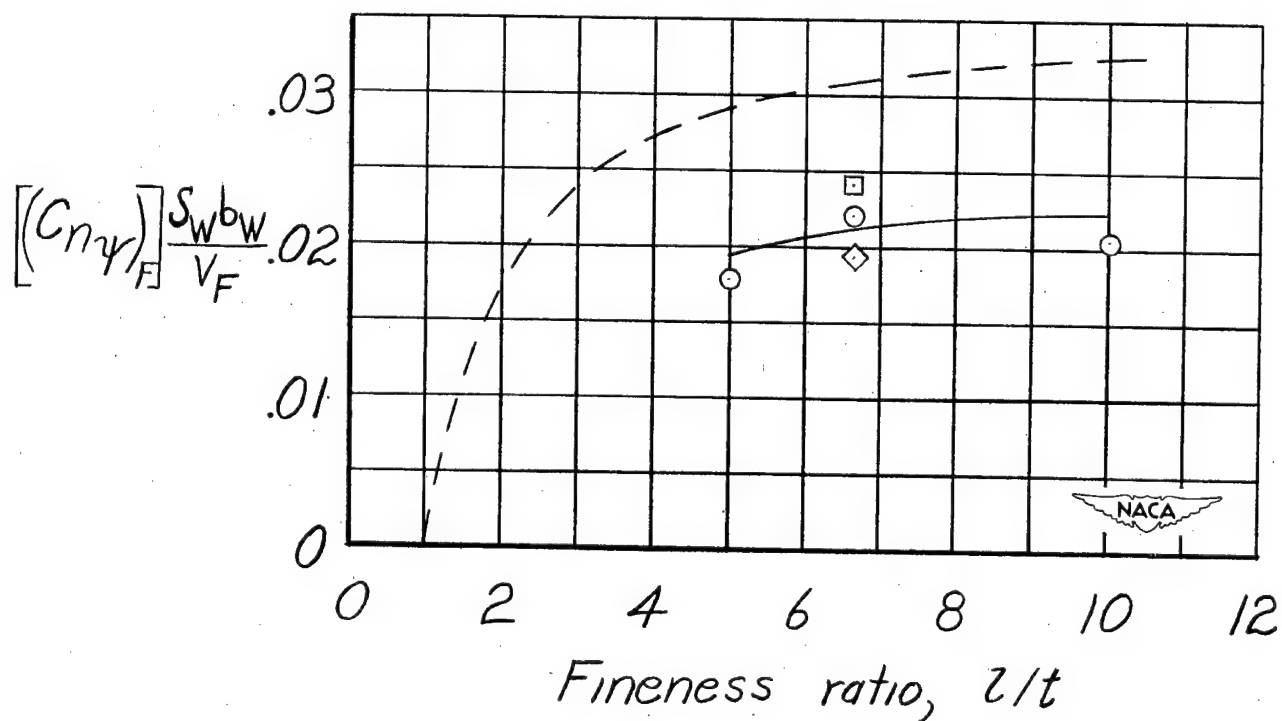


Figure 16.- Summary of fuselage contributions to  $C_{Y\psi}$  and  $C_{n\psi}$ .  $\alpha = 0^\circ$ .

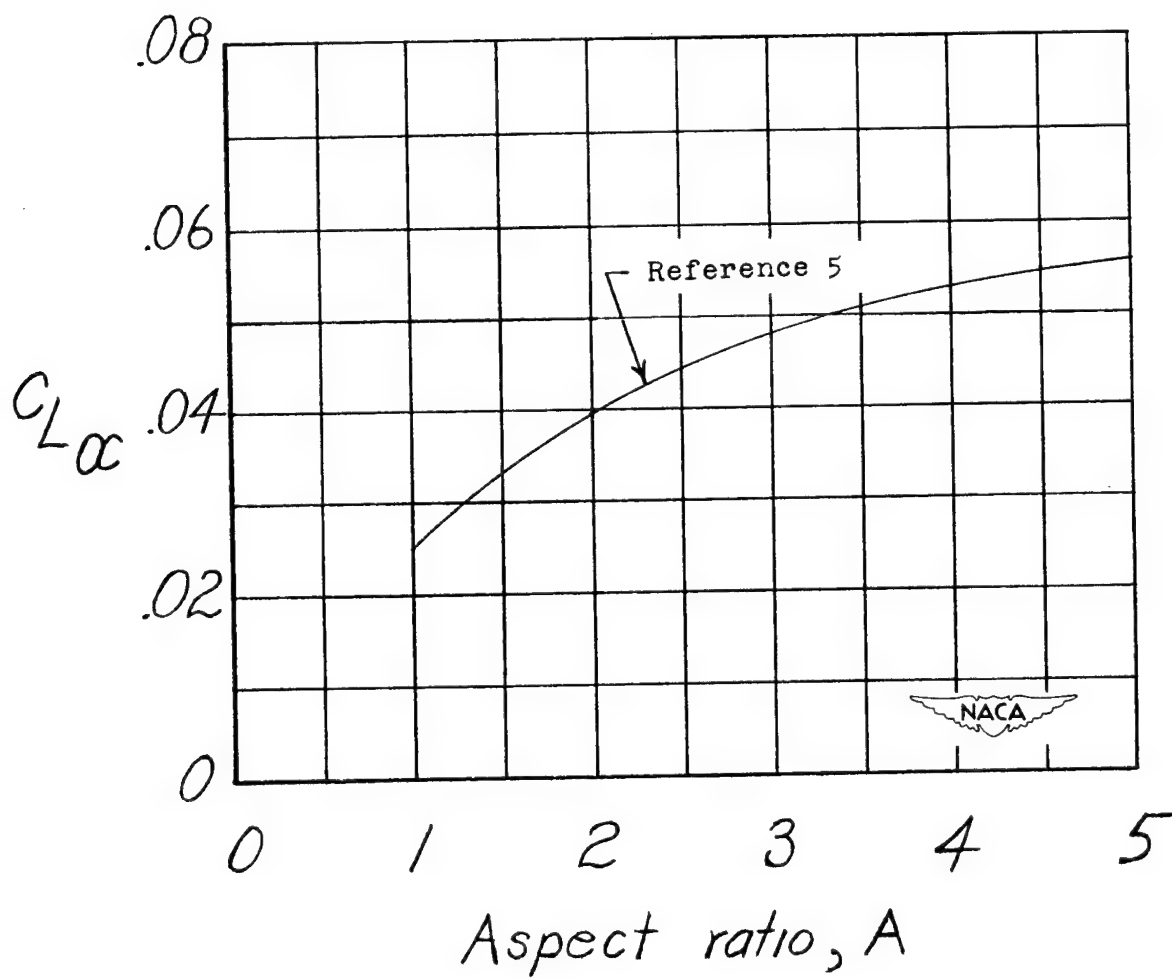


Figure 17.- Variation of lift-curve slope with aspect ratio for  $45^\circ$  sweptback wings with taper ratio 0.6.

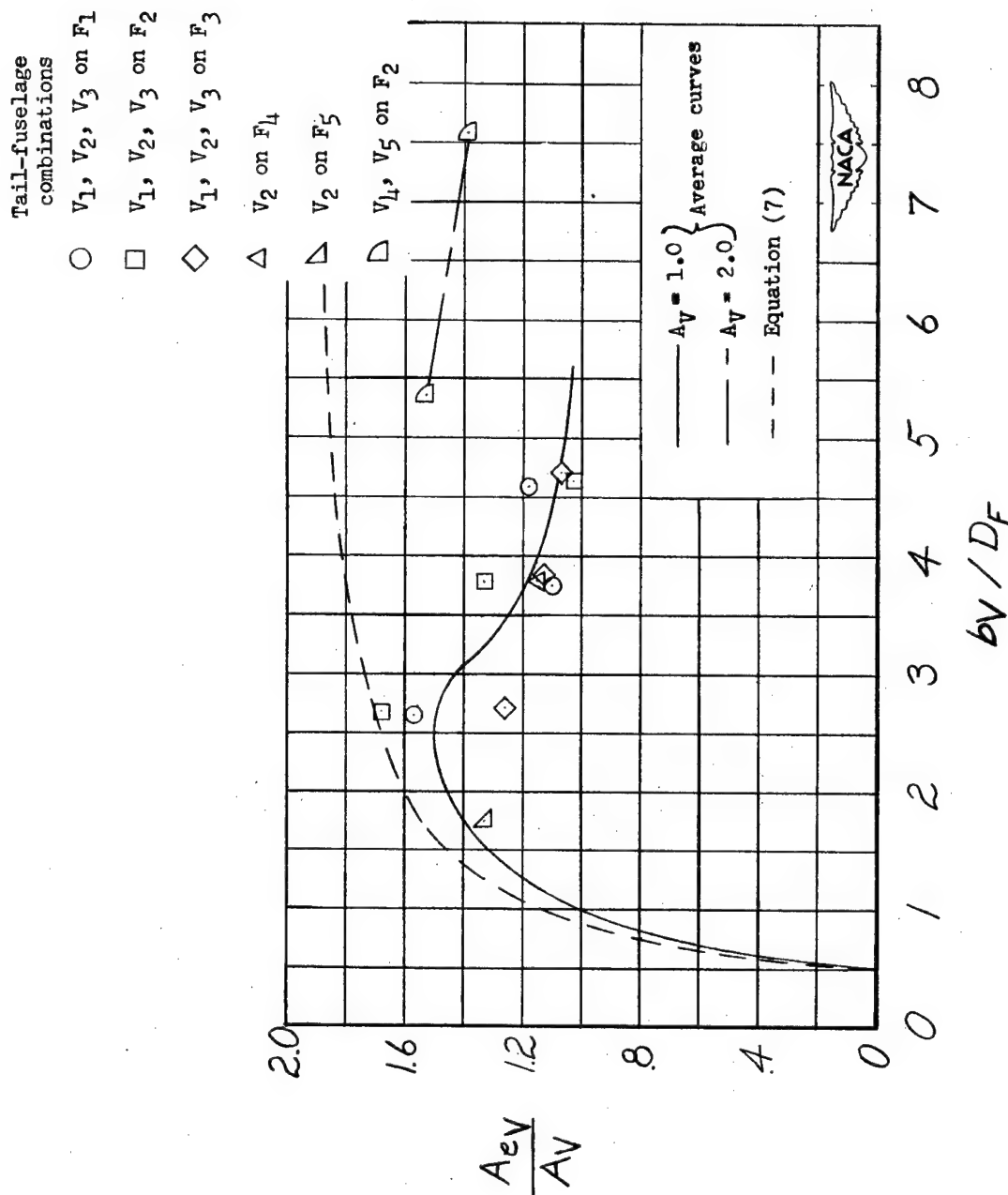


Figure 18.- Effective aspect ratio of vertical tails as influenced by the fuselage.  $\alpha = 0^\circ$ .

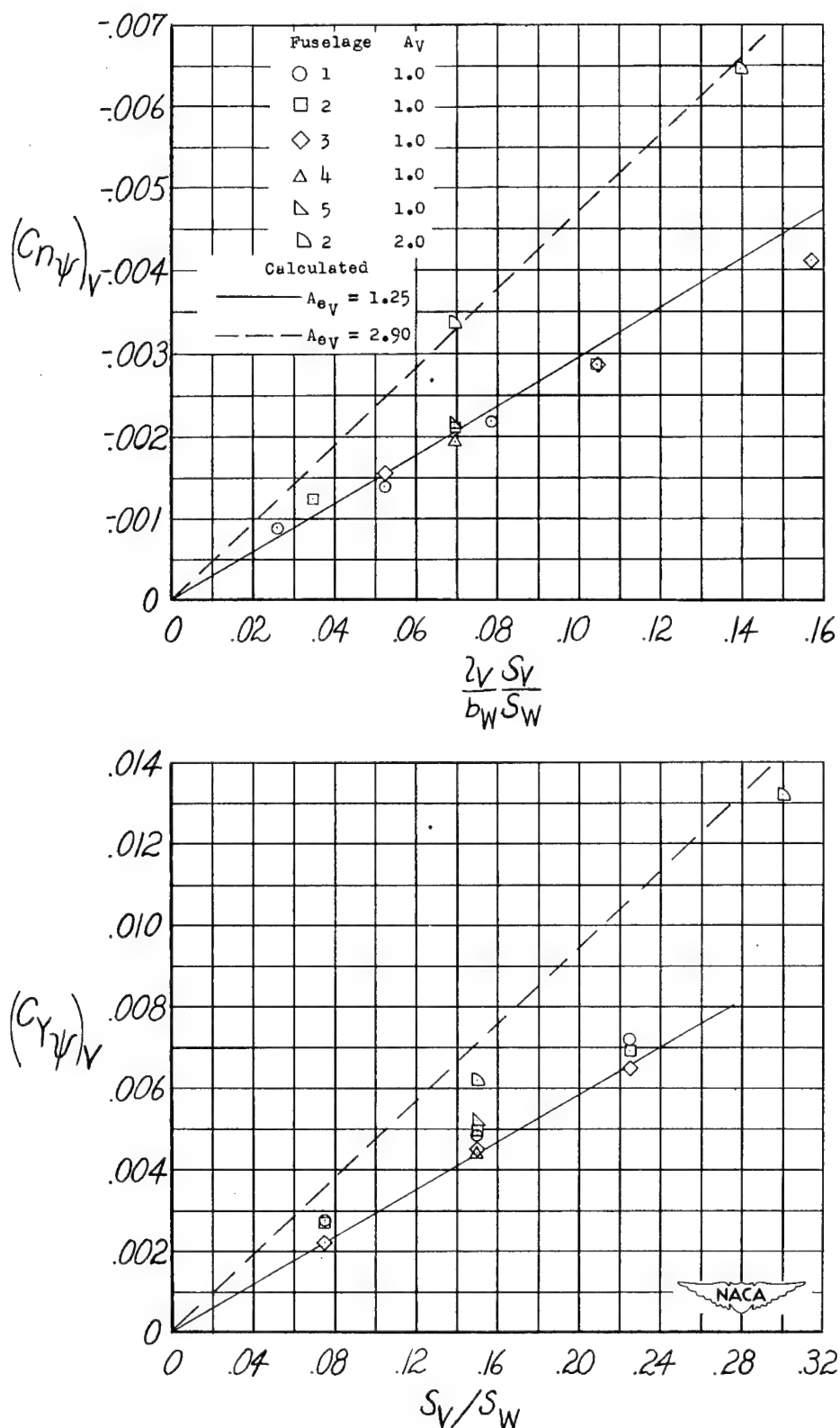


Figure 19.- Effect of tail area and tail length on vertical-tail contribution to  $C_{Y\psi}$  and  $C_{n\psi}$ .  $\alpha = 0^\circ$ .



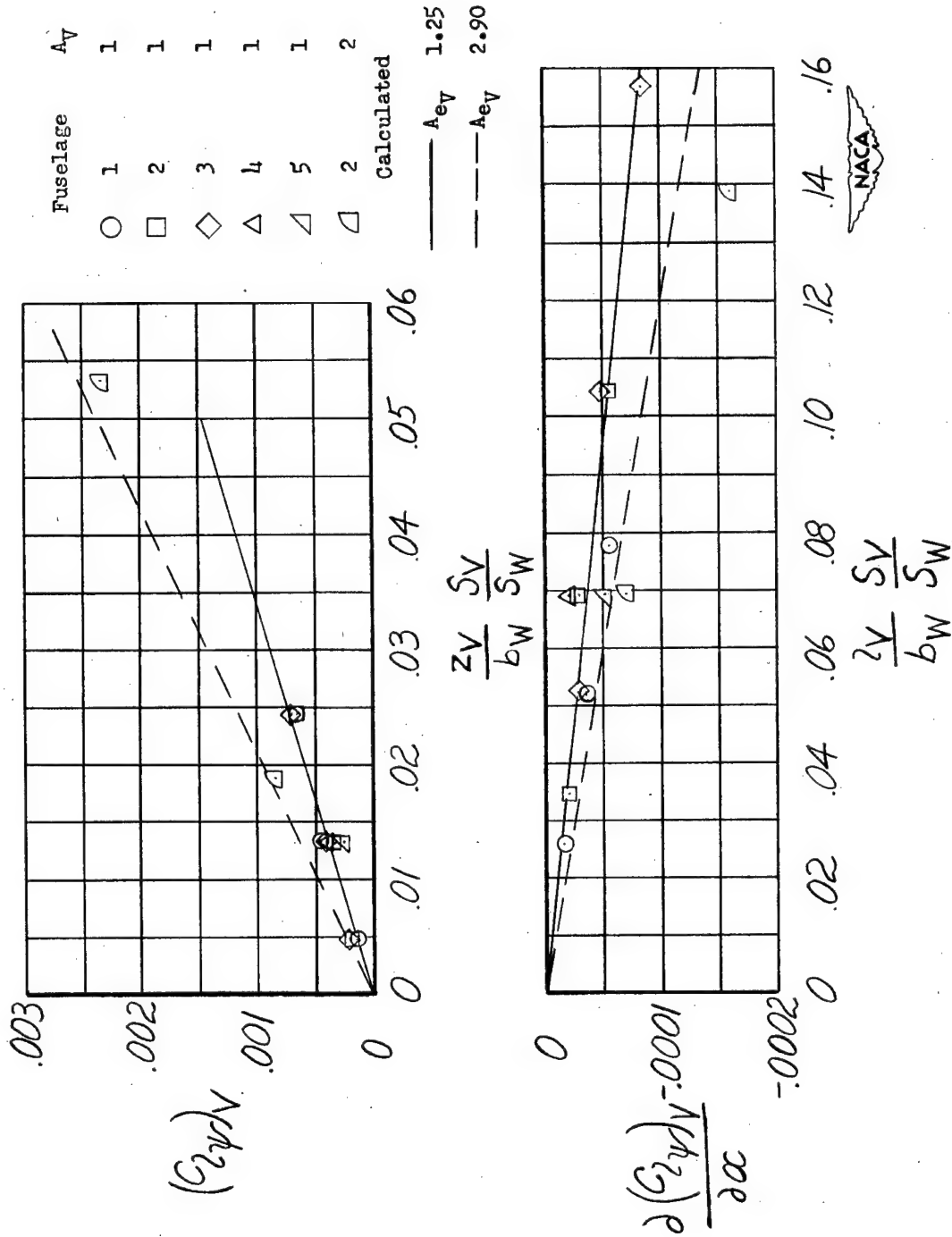


Figure 20.- Effect of tail area and length on the vertical-tail contribution to  $C_{l\psi}$ .  $\alpha = 0^\circ$ .

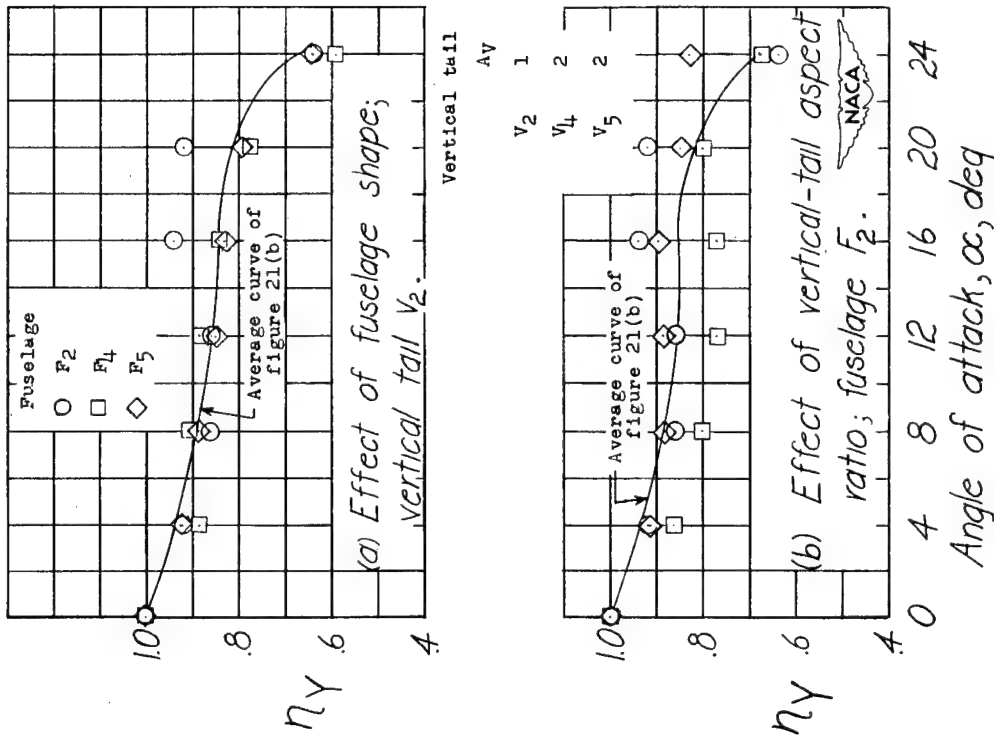


Figure 22.- Effect of fuselage shape and vertical-tail aspect ratio on the angle-of-attack correction to the vertical-tail contribution to  $C_{Y\psi}$ .

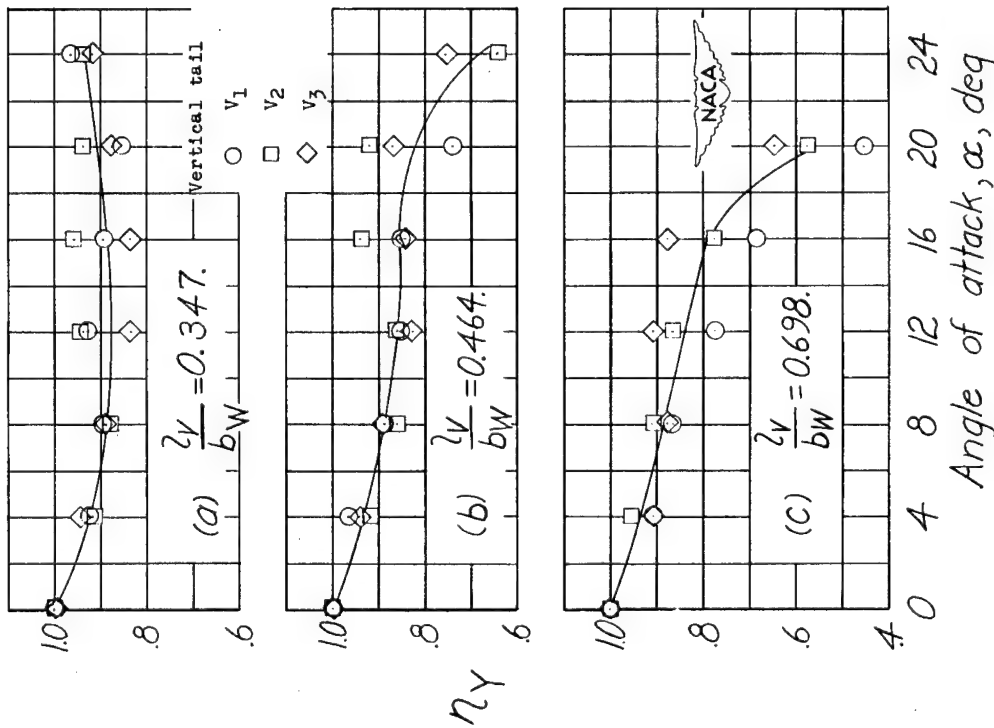


Figure 21.- Effect of tail area and length on the angle-of-attack correction to the vertical-tail contribution to  $C_{Y\psi}$ . Circular-arc fuselages.

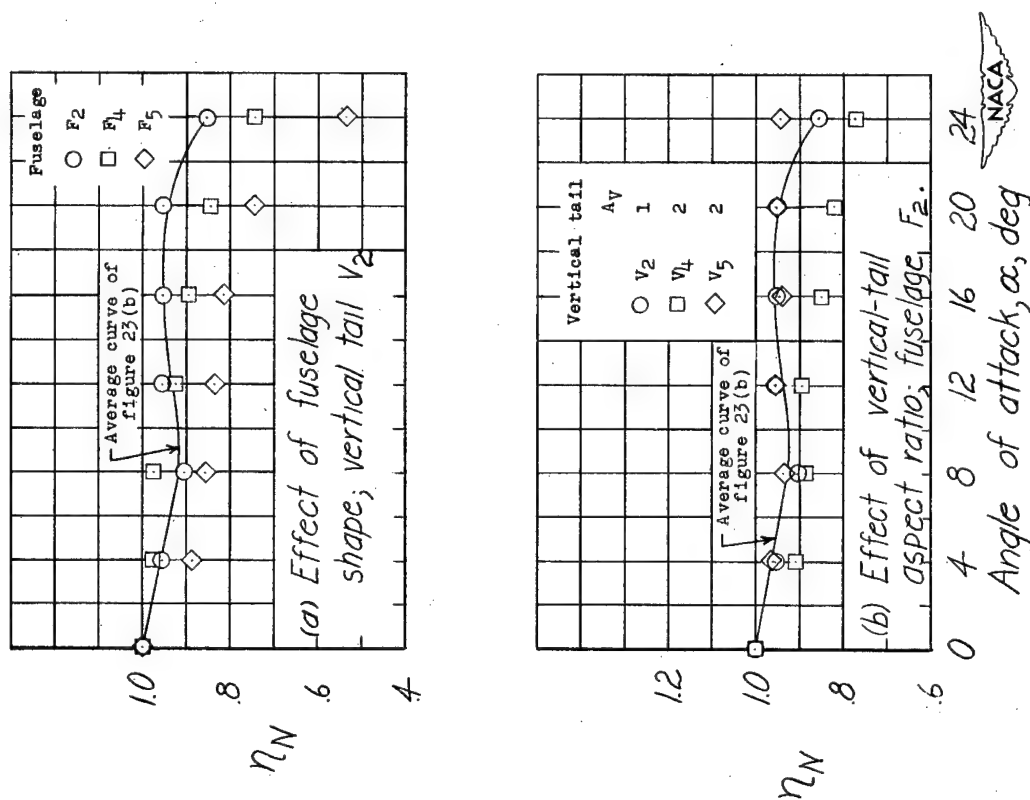


Figure 24.- Effect of fuselage shape and vertical-tail aspect ratio on the angle-of-attack correction to the vertical-tail contribution to  $C_{n\psi}$ .

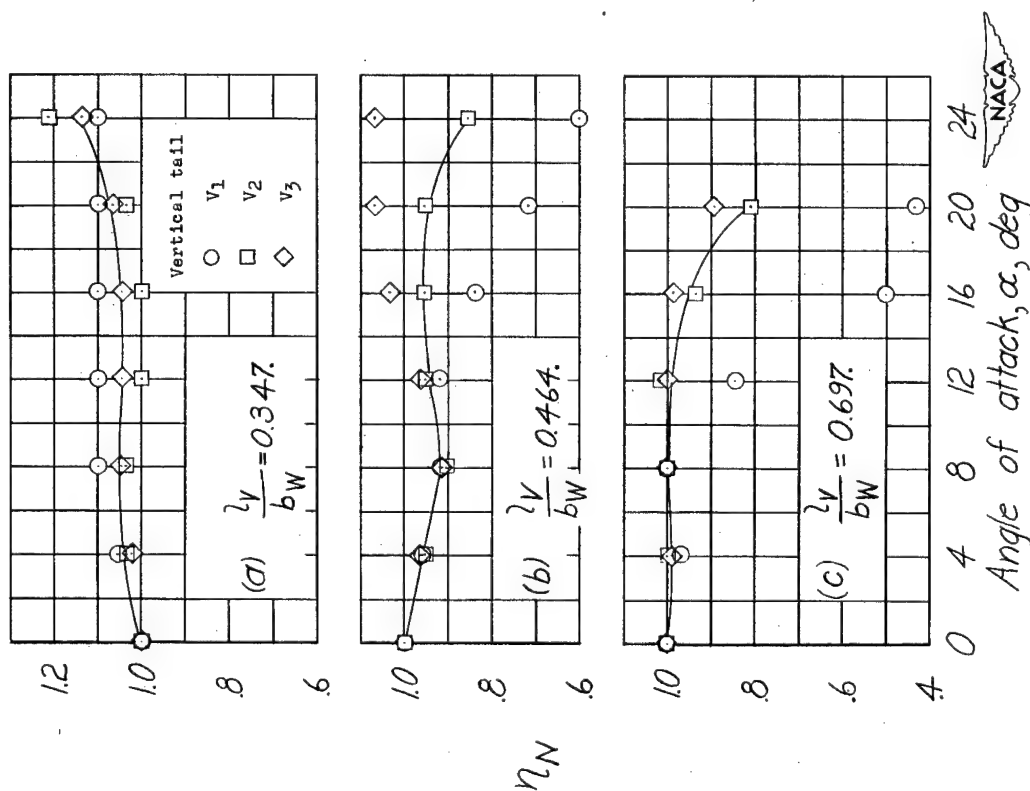


Figure 23.- Effect of tail area and length on the angle-of-attack correction to the vertical-tail contribution to  $C_{n\psi}$ . Circular-arc fuselages.

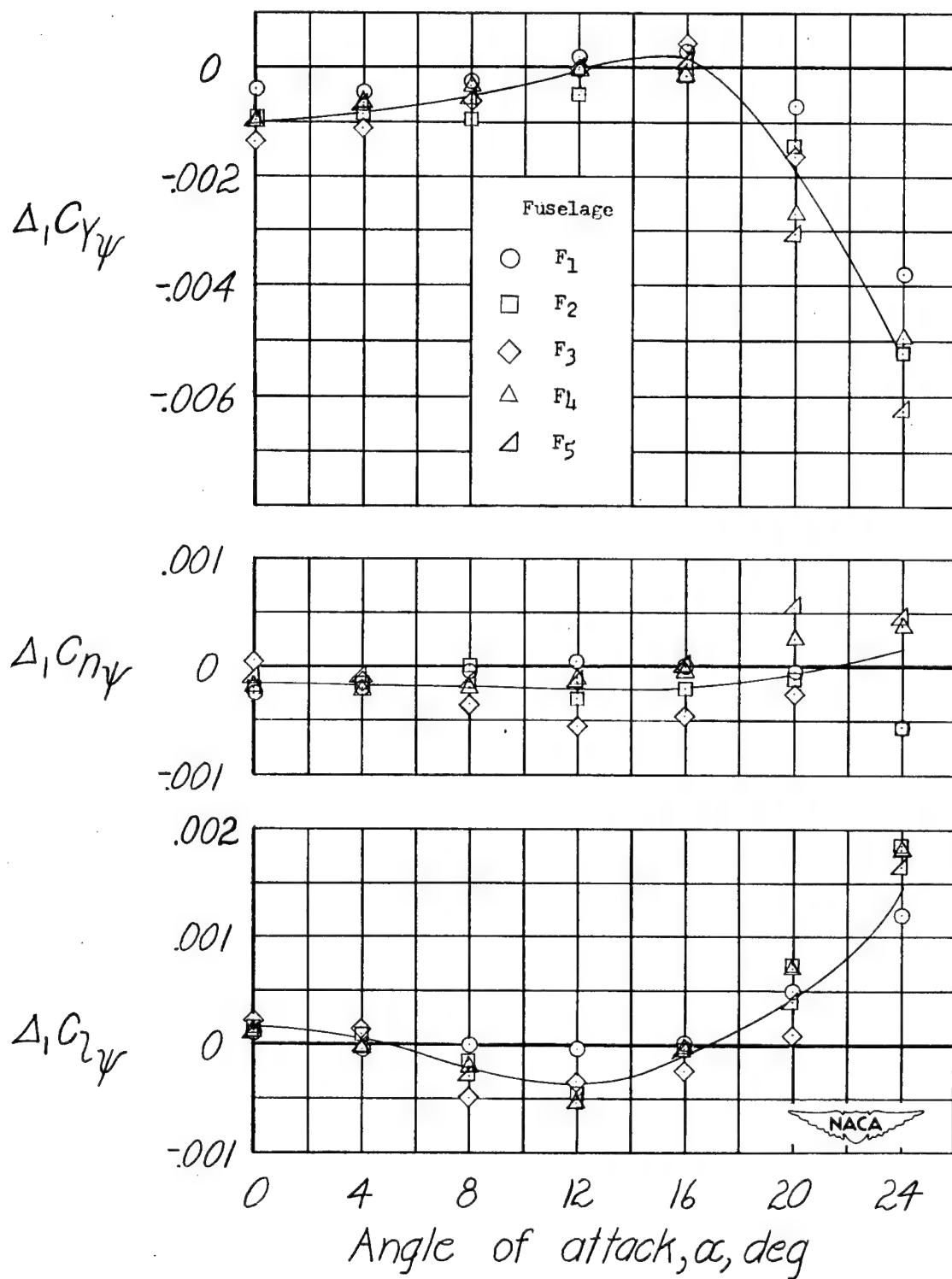


Figure 25.- Variation of increments of  $C_{Y\psi}$ ,  $C_{n\psi}$ , and  $C_{l\psi}$  caused by wing-fuselage interference with angle of attack.

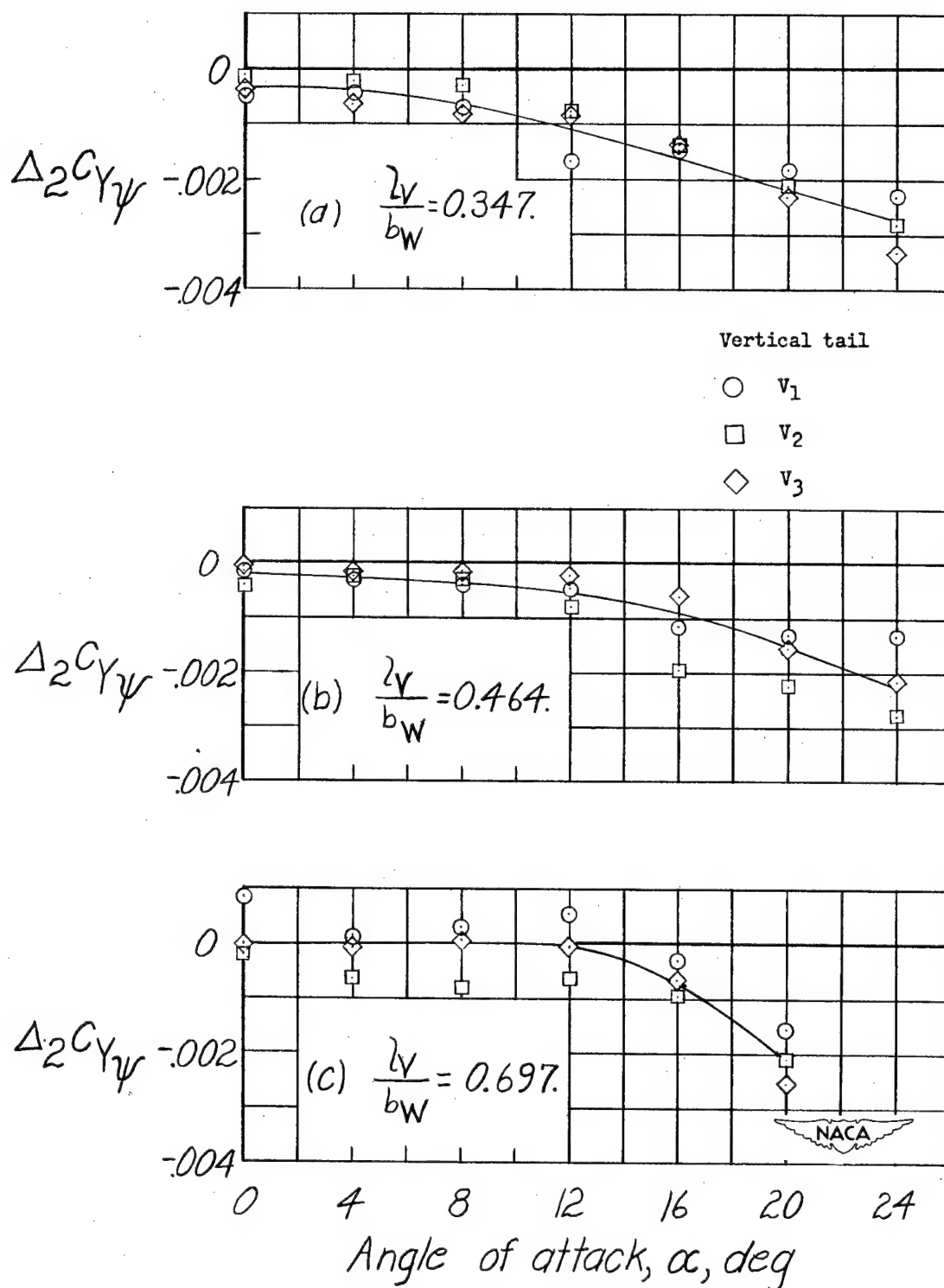


Figure 26.- Effect of the tail area and length on the increment of  $C_{Y\psi}$  caused by wing-fuselage interference on vertical-tail effectiveness. Circular-arc fuselages.

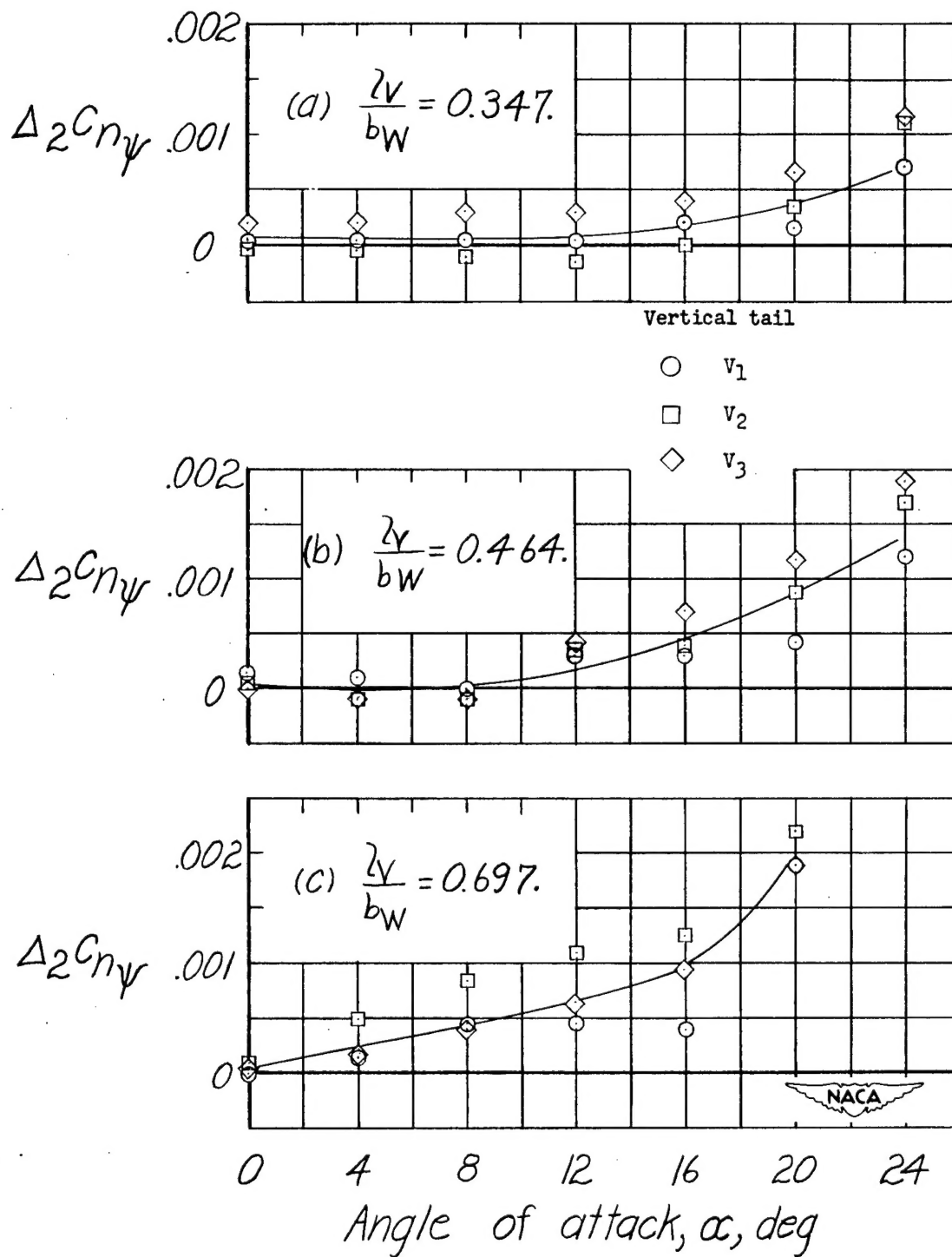


Figure 27.- Effect of tail area and length on the increment of  $C_{n\psi}$  caused by the wing-fuselage interference on the vertical-tail effectiveness. Circular-arc fuselages.

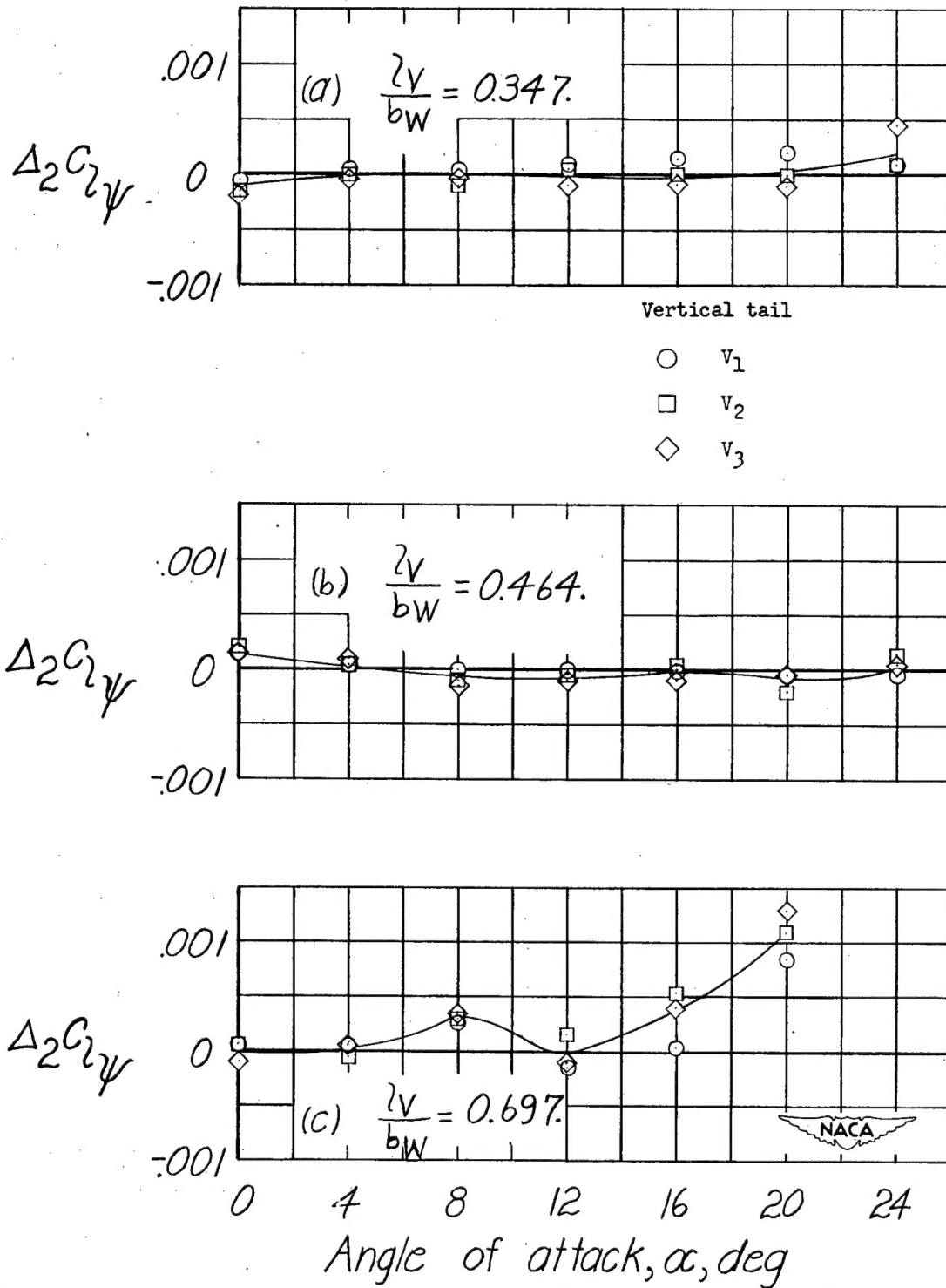


Figure 28.- Effect of tail area and length on the increment of  $C_{L_{\psi}}$  caused by the wing-fuselage interference on vertical-tail effectiveness. Circular-arc fuselages.

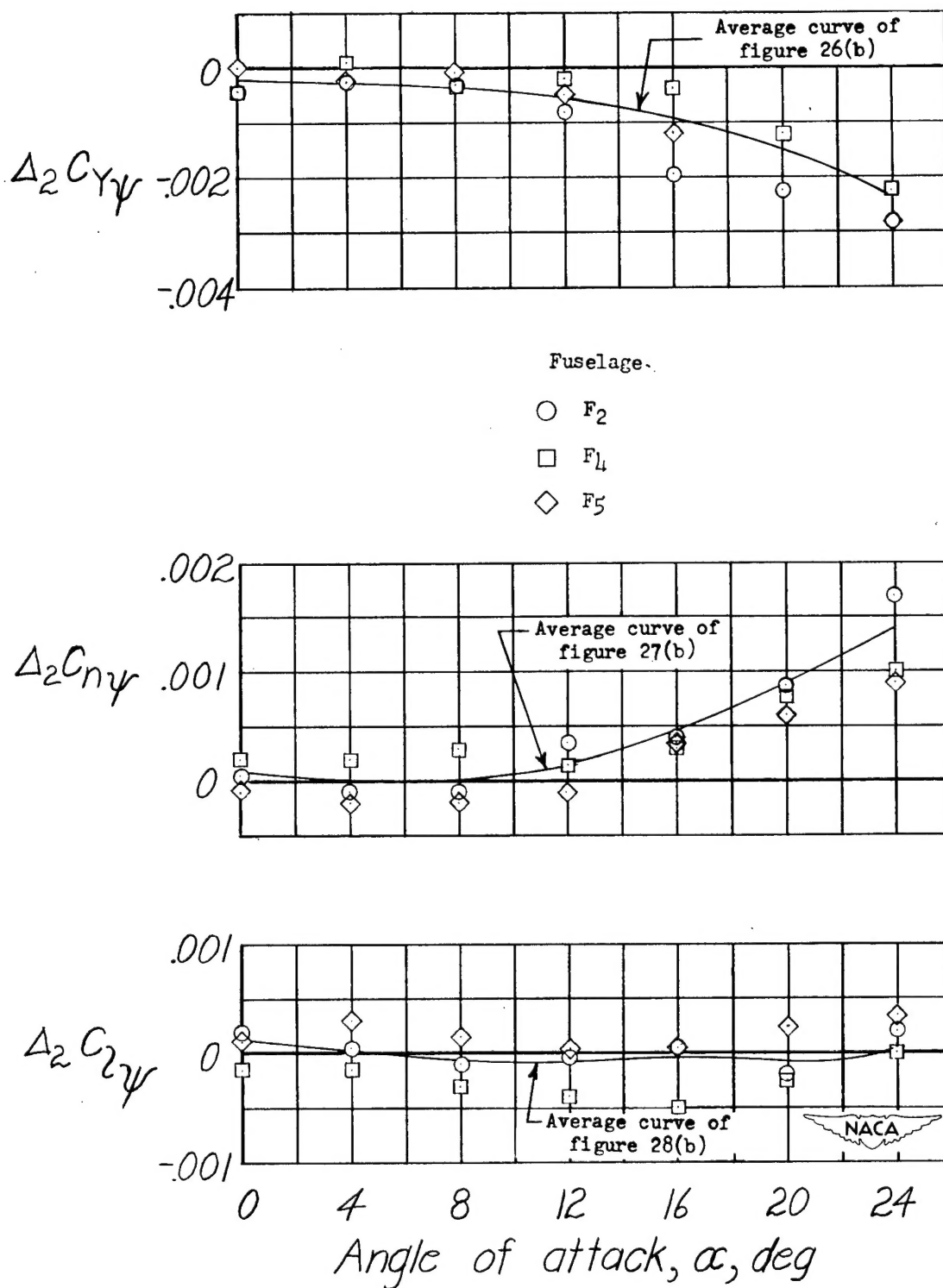


Figure 29.- Effect of fuselage shape on the increments of  $C_{Y\psi}$ ,  $C_{n\psi}$ , and  $C_{l\psi}$  caused by the wing-fuselage interference on the vertical-tail effectiveness. Vertical tail  $V_2$ .



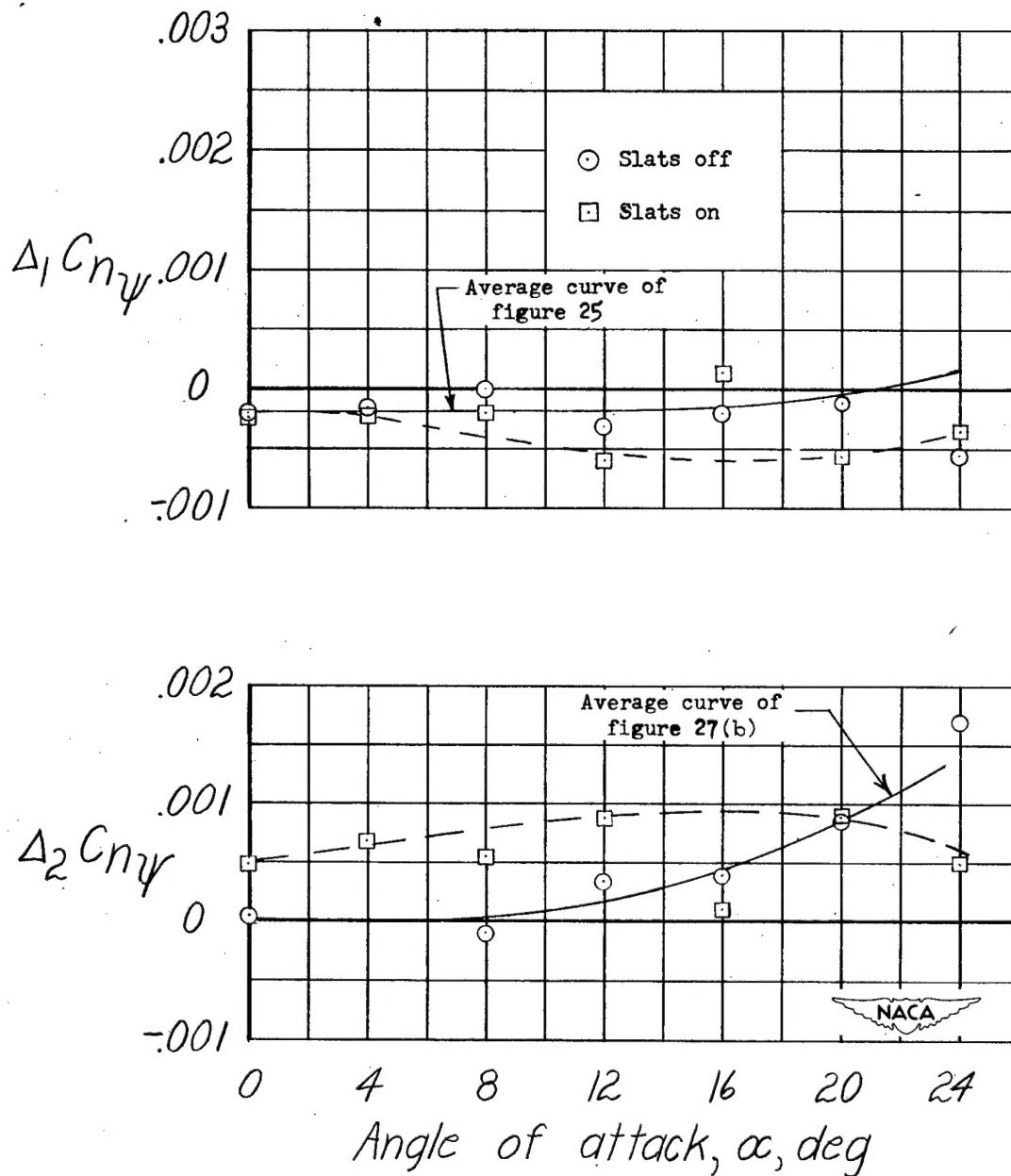


Figure 30.- Effect of leading-edge slat on interference increments.  
 Fuselage  $F_2$ ; vertical tail  $V_2$ .